TOPICAL REVIEW

Photonic surface waves on metamaterial interfaces

IOP Publishing Journal of Physics: Condensed Matter

J. Phys.: Condens. Matter **29** (2017) 463001 (20pp) https://doi.org/10.1088/1361-648X/aa8bdd

Topical Review

Photonic surface waves on metamaterial interfaces

O Takayama[1], A A Bogdanov[2] and A V Lavrinenko[1,2]

[1] Department of Photonics Engineering, Technical University of Denmark, Ørsteds Plads, Building 343, DK-2800 Kgs. Lyngby, Denmark
[2] Department of Nanophotonics and Metamaterials, ITMO University, 14 Birjevaja line V.O., St. Petersburg 199034, Russia

E-mail: alav@fotonik.dtu.dk

Received 8 June 2017, revised 8 September 2017
Accepted for publication 12 September 2017
Published 20 October 2017

Abstract

A surface wave (SW) in optics is a light wave, which is supported at an interface of two dissimilar media and propagates along the interface with its field amplitude exponentially decaying away from the boundary. Research on surface waves has been flourishing in the last few decades due to their unique properties of surface sensitivity and field localization. These features have resulted in applications in nano-guiding, sensing, light-trapping and imaging based on near-field techniques, contributing to the establishment of nanophotonics as a field of research. Up to now, a wide variety of surface waves has been investigated in numerous material and structure settings. This article reviews the recent progress and development in the physics of SWs localized at metamaterial interfaces, as well as bulk media in order to provide broader perspectives on optical surface waves in general. For each type of surface wave, we discuss the material and structural platforms. We mainly focus on experimental realizations in the visible and near-infrared wavelength ranges. We also address existing and potential application of SWs in chemical and biological sensing, and experimental excitation and characterization methods.

Keywords: metamaterials, surface waves, dispersion

(Some figures may appear in colour only in the online journal)

1. Introduction

For decades the guiding of light in optics has been conducted based on the same principle: when light travels in a medium with a refractive index higher than that of the ambient media (claddings). In this manner, light propagates within the high refractive index region (core), being totally reflected at its interfaces. Such an operation requires that a light beam bounces back and forward between the interfaces for waveguiding. This principle is the same for optical fibers and planar integrated optical circuits. Typical photonics devices complying with high operational frequencies suffer from the notorious diffraction limit, which does not allow shrinkage of the optical components' footprints to those of the electronic counterparts. One of the high-potential perspectives to overcome this strict limitation is associated with optical surface waves (SWs) [1]. A SW is a propagating electromagnetic mode supported at an interface between two dissimilar media. SWs are typically strongly localized exhibiting the maximum of the field's amplitudes in the vicinity of the interface and exponentially decaying away from it [1]. There are various types of SWs based on different material settings characterized by

permittivity or permeability features. Known types of SWs to date can be categorized as [3]:

1. Surface plasmons (require negative permittivity of one of the media in contact) [4]
2. Magnetic plasmons (require negative permeability of one of the media in contact) [5]
3. Dyakonov surface waves (require linear anisotropy of at least one of the media in contact) [6]
4. Nonreciprocal surface waves on optically active or gyrotropic materials (require circular anisotropy of one of the media in contact) [7]
5. Tamm waves or optical Tamm states (require periodic permittivity of one of the media truncated by the interface) [8] and Bloch surface waves (require periodic permittivity of one of the media along the interface)
6. Surface solitons (require nonlinear permittivity of one of the media) [9].

Of course, this is not a complete classification of SWs. There are many other specific types of SWs such as surface phonon-polaritons [10–13], surface exciton-polaritons [14, 15], 2D plasmon waves [16–19], Dyakonov plasmons [20–22], topological surface waves and edge states [23–25] and many others. The most well-known example of optical surface waves is a surface plasmon polariton (type 1 SW in the categorization scheme above) supported at the interfaces between metals and dielectrics. It has been actively studied since the early XX century [26]. However, some SWs are quite new and are being actively studied now.

This review is organized as follows. First, we elaborate the straightforward classification of the known types of surface waves considering the permittivity and permeability tensors of media and structures forming the interface. This classification encompasses electrical and magnetic surface plasmon polaritons, surface waves localized at the interfaces of hyperbolic media, and nonreciprocal surface waves on gyrotropic materials. Some of these SWs are supported on the 'metamaterial' interfaces. Metamaterial can be briefly defined as an artificially engineered periodic (or random) medium or structure whose periodicity (or characteristic length parameter) has a much smaller pitch than the wavelength and therefore can be considered as a homogenized medium characterized by an effective permittivity and permeability. The full potential of such SWs has not been fully exploited. To date, SWs types 1 to 6 have been investigated mostly individually due to challenges in acquiring the necessary nomenclature of the materials' properties. Nevertheless, nowadays new kinds of surface waves are created by hybridization of different basic types of SWs. Thereby metamaterial structures play a pivotal role to support the realization of unconventional combinations of permittivities and permeabilities. The possibility of engineering effective parameters of metamaterials opens up new perspectives in photonics, primarily because they can provide unusual optical properties which natural materials do not have [27–29]. The role of metamaterials is twofold: (1) to facilitate each individual SW (according to the classification given above) and (2) to hybridize individual SWs creating new types of combined SWs. Regarding (1), often some photonic surface waves exist on natural materials, however, only in a certain wavelength range. Therefore, metamaterials play a crucial role in extending the ranges of existence beyond those feasible with natural materials. Here, waves such as Dyakonov plasmons on hyperbolic media can be addressed. Throughout the review, we refer to surface waves as 'propagating electromagnetic waves that are supported at an interface of two dissimilar media and propagate along the interface with its field amplitude exponentially decaying away from the boundary.' These propagating surface waves are different in nature from localized surface plasmons or particle plasmons, therefore we do not touch on localized surface plasmons or any other non-propagating boundary states or resonances.

Furthermore, we extend the category of metamaterials on to photonic crystal structures, whose periodicities are of the order of the wavelength unlike the conventional definition of metamaterials, and consider surface waves on photonic crystals, which are localized due to the photonic bandgaps of the structures. In particular, we analyze optical Tamm waves, Bloch surface waves, Tamm-plasmons and Dyakonov–Tamm plasmons. We also describe nonlinear surface waves, surface solitons and nonlinear Dyakonov surface waves supported at the interface with nonlinear materials. We finalize the review by introducing surface waves on 2D materials and metasurfaces, which have been rapidly emerging in recent years and may not be categorized into the above-mentioned principle types due to an absence of bulk properties. We conclude the paper with a summary of the main features of the reviewed surface waves and an outlook of their current and future applications.

2. Surface waves on the interface of homogeneous media and their classification

In this section, we consider SWs supported on homogeneous media characterized by constant permittivities and permeabilities without any spacial variations. This includes metamaterial structures composed of more than one periodic material whose periodicities are much smaller than the wavelength under consideration so that the whole structure can be treated as a homogenized medium with effective material parameters. Some surface waves can be supported on isotropic media. However, many SWs are hosted on anisotropic media, whose permittivity and permeability are expressed in tensorial forms.

2.1. Surface plasmons (note: require negative permittivity of one of the media)

Surface plasmon polaritons (SPPs) are collective synchronized oscillations of free electrons in the conducting bands of metals and electromagnetic fields at the vicinity of the interface between conductive material (f. e. noble metal) and dielectric (air) [4]. These oscillations can occur with optical frequencies up to the plasma frequency of the metal, which is determined by the free electrons' concentration and effective mass of electrons [30]. SPPs are bound to the interface of materials with a high electron density; that is they are surface

waves, and this is their distinct difference to unbounded light waves. The magnetic field of SPPs is parallel to the plane of the interface; and in other words, SPPs are TM-polarized modes only.

Assuming a nonmagnetic material with unity permeability ($\mu = 1$), the normalized propagation constant (component of the wavevector in the direction of propagation) or effective mode index of a surface plasmon polarition, N_{SP}, is given by

$$N_{SP} = k_{SP}/k_0 = ((\varepsilon_d \varepsilon_m)/(\varepsilon_d + \varepsilon_m))^{1/2}, \quad (1)$$

where k_{SP} is the propagation constants of the surface plasmon polariton, k_0 is the relevant vacuum wavenumber, ε_d and ε_m are the dielectric functions of the dielectric and metal layers, respectively [31]. For the propagation constant to be real the expression under the square root in equation (1) must be positive. While ε_m is negative, the two media have to satisfy an additional condition $\varepsilon_d < |\varepsilon_m|$. In other words, one of the materials at the interface has to be dielectric with a positive permittivity, and another often termed as a *plasmonic* material has to possess a negative permittivity with a larger absolute value. Plasmonic materials at visible and near-infrared wavelengths are typically noble metals such as silver, gold, copper, and aluminum. However, for near-infrared wavelengths and beyond, there is a wide variety of alternative plasmonic materials, such as transparent conductive oxides (TCO): indium tin oxide (ITO), aluminum-doped zinc oxide (AZO), gallium-doped zinc oxide (GZO), and the group of nitrides, for example, titanium nitride (TiN) and zirconium nitride (ZrN) [32–34]. For mid-infrared wavelengths $\lambda > 2$ μm, there are additional options of materials, such as doped semiconductors [35]. Moreover, negative permittivity ranges also occur in certain polar materials, polaritonic crystals and 2D materials around the phonon-polariton resonances [36–39].

Normally a propagation constant of SPPs expressed in equation (1) $k_{SP} > k_0$, so a light wave does not have sufficient momentum for efficient coupling with the SPP mode merely by shining light from air onto the metal surface due to the momentum's mismatch. The excitation and observation methods of SPPs are summarized in figure 1. In order to suffice the propagation constant it is possible to illuminate the interface through an optically dense material, e.g. through a prism, as illustrated in figures 1(a)–(c). Such an excitation and observation scheme is known as the Otto configuration for the case where there is an air gap between the prism and the metal [40], and the Kretchmann configuration when the metal layer is placed directly on the prism surface [41]. In the prism with refractive index n_p the parallel (to the interface) component of the normalized wavevector is expressed by

$$N_{\parallel} = k_{\parallel}/k_0 = n_p \sin(\phi), \quad (2)$$

where ϕ is the angle of incidence. When the parallel component of the wavevector of a light wave in a prism coincides with that of SPPs, efficient coupling of external light to a surface mode takes place. As a consequence, reflected light for this particular angle of incidence should be less intensive, thus allowing observation of the surface waves in terms of the wavelength and angle of incidence (corresponding wavevector). This technique allows one to map the propagation constant of the plasmon modes in terms of the wavelength, that is, to depict the dispersion diagram (ω versus β) of the SPPs. A leakage radiation microscope is also based on the same principle. It is used for the observation of plasmons in the wavevector (reciprocal) and real spaces for visible to near-infrared wavelengths [31]. However, the maximum wavevector allowed in these prism coupling schemes is limited by the refractive index of the prism, n_p. Therefore, one can only observe surface plasmons with propagation constant $N_{SP} < n_p$. Typically, materials for prisms are SiO_2 ($n_p \approx 1.5$) for the visible to near-infrared, ZnSe ($n_p \approx 2.5$) for the visible to mid-infrared, Si ($n_p \approx 3.5$) for the near- to mid-infrared, and Ge ($n_p \approx 4.0$) for the mid-infrared wavelength regions. SWs on metamaterials and 2D materials may possess extremely large wavevectors and, therefore, observing them by the prism coupling scheme may be difficult.

In order to match wavevectors larger than that provided by a conventional prism, a grating coupler and decoupler can be used as shown in figure 1(d). The normalized propagation constant generated by the grating, k_g, is mainly dictated by the pitch, Λ, and is expressed by

$$k_g = n_s \sin(\phi) + m\lambda/\Lambda (m = 1, 2, 3, ...), \quad (3)$$

where n_s is the refractive index of the superstrate of the grating and λ is the wavelength. A large wavevector k_g can be generated by designing the pitch of the grating, Λ as opposed to the wavelength. Moreover, a single subwavelength scatterer (nanoparticle or nanoantenna) can be used to excite plasmons as illustrated in figure 1(e). Light scattered by the nanoparticle contains various wavevectors, and some of them can match the wavevector of the SWs. Thus the excitation of SPPs can occur, although the coupling efficiency of a single scatterer may not be as high as that of the grating coupler. However, the use of resonant high-index dielectric nanoparticles can simultaneously provide high efficiency and directivity of SPP excitation [1]. Scatterers are also used for a scattering-type scanning near a field optical microscope (s-SNOM), also known as aperture-less near-field scanning optical microscopy [42]. A s-SNOM is based on the sharp metal tip of an atomic force microscope (AFM) cantilever and functions both in excitation and detection modes. By scanning the metallic tip over the sample surface, s-SNOM can probe the local electric fields on the sample surface and image a 2D spectroscopic map with super-resolution quality (up to 20 nm resolution depending on the tip shape) of the surfaces of various materials and nanostructures. Combined with an external light source with the wavelength of interest, s-SNOM can operate in a wide range of wavelengths from visible to mid-IR and even up to the THz region. S-SNOMs have been used for the observations of nano-optical phenomena, such as surface plasmons in graphene [43]. A point source (such as quantum dots and fluorescent dyes) that emits light can excite surface waves too. For such an action a point light source needs to be placed near the interface, and detection can be conducted in the wavevector space by a leakage radiation microscope [44].

The simple end-fire coupling technique (known in fibre optics as butt coupling) can be used to excite SWs and waveguide modes by focusing external light on the edge of a

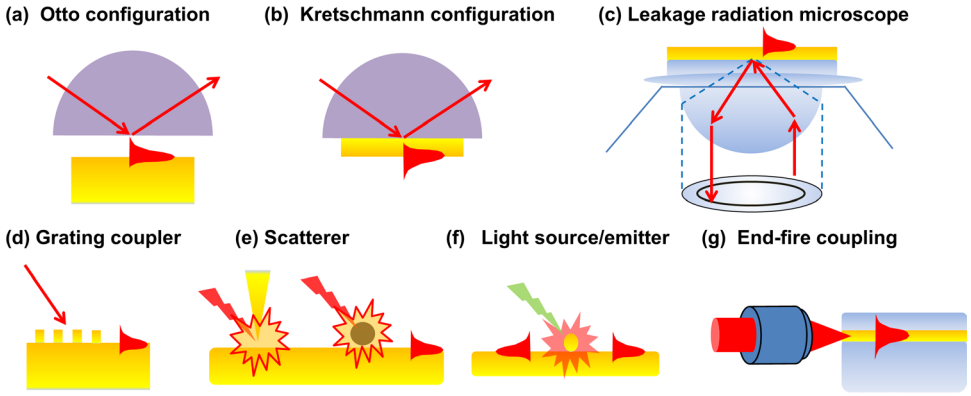

Figure 1. Excitation and observation of surface waves. Prism coupling scheme, (a) Otto and (b) Kretschmann configurations. (c) Leakage radiation microscope.(d) Grating coupler, (e) tip and scatterer, (f) point light source such as quantum dots and fluorescent molecules. (g) End-fire coupling.

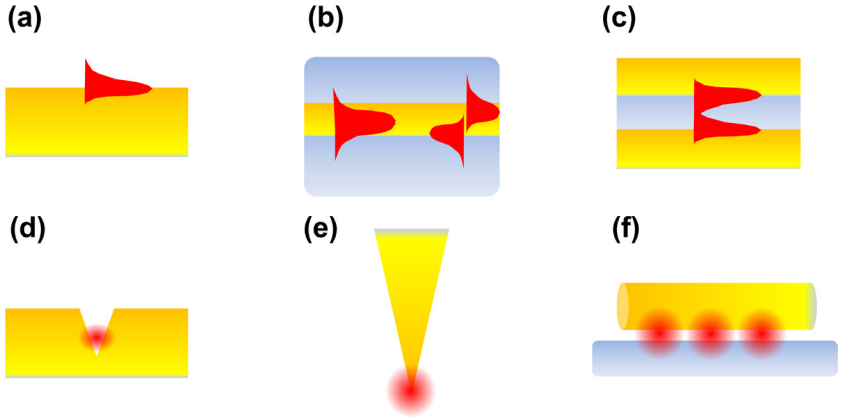

Figure 2. Configuration of plasmon polaritons. (a) Planar metal-dielectric interface. (b) Dielectric-metal-dielectric. (c) Metal-dielectric-metal. (d) Metallic gap. (e) Metallic wedge. (f) Metal nanowire.

waveguide or structure that supports SWs [45]. The focusing of light is conducted by a microscope objective lens or optical fibre pointing the edge of the structure as shown in figure 1(g). Its coupling efficiency is mainly determined by the overlap of the focused beam spot and the field profile of the SWs at the edge of the waveguide structure, as well as by the quality of the edge. Detection of excited SWs can also be performed in the same way by placing a microscope objective or optical fibre to collect light coming out at the output end of the structure. Note that the excitation and observation techniques discussed in this section are in general applicable not only to SPPs, but to other types of surface waves and guided modes as well.

Surface plasmon-polaritons are supported not only at planar interfaces, but also in a wide variety of geometries, such as dielectric-loaded waveguides, dielectric-metal-dielectric, metal-dielectric-metal structures [46], metal slits or gaps, metallic tips or wedges, metal nanowires [47] as illustrated in figure 2. More extensive reviews on plasmonics can be found in [1, 4, 48, 49].

Since plasmon resonances are sensitive to the state of the interface, especially to the refractive index of the dielectric material surrounding a thin metal film, chemical sensors can be constructed by detecting the refractive index variation of the dielectric medium [50]. A change of the refractive index can be induced by some chemical agents and results in a change of the SPP propagation constant, see equation (1), which can be detected as the variation of the incident angle or shift of the SPP resonance in the wavelength domain. It was reported that a SPP-based sensor is capable of detecting a change in the refractive index of the order of 10^{-7} refractive index units (RIU). Such sensors were demonstrated for the detection of pesticides, pollutants, explosives, bacteria, viruses, toxins, allergens, and so forth [51]. The sensing applications of plasmons are not restricted to the refractive index sensing in the visible and near-infrared wavelength regions, but also used for sensing based on the enhancement of the vibrational absorption of molecules in the mid-infrared range [52, 53].

Apart from sensing applications, the capability of SPPs to localize electric field at the vicinity of the metal surface within the subwavelength scale of tens of nanometers [54] leads to such applications as waveguides [55, 56], switches [57], enhancement of photon-matter effects including nonlinear effects [58], and thermal management by designed metallic nanostructures generating heat localized in the radius on the order of hundreds of nanometers [59] around the nanoheater. Dielectric-metal-dielectirc waveguides can support the SPP modes at THz frequencies while having of a subwavelength thickness and providing almost perfect optical confinement [60]. This advantage of dielectric-metal-dielectirc waveguides is used in commercial THz quantum cascade lasers [61]. Among various metallic nanostructures that support SPPs,

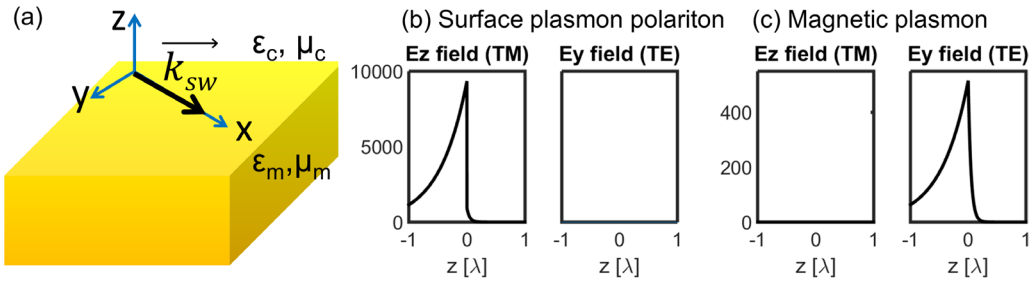

Figure 3. Difference of the field profile between the surface plasmon polarition and magnetic plasmon. (a) Geometry under consideration with an interface between air ($\varepsilon_c = \mu_c = 1, z > 0$) and material with ε_m, μ_m, $z < 0$. Note that the wavevector of the surface waves either the surface plasmon polariton or magnetic plasmon is parallel to the x-axis. The norm of the fields for (b) surface plasmon polariton with $\varepsilon_m = -10$, $\mu_m = 1$ and (c) magnetic plasmon with $\varepsilon_m = 1$ and $\mu_m = -10$.

metal tips and antennas have been investigated for the concentration of fields at the desired spot [62]. Light cannot be focused in the dimensions below the diffraction limit, which determine the maximum resolution of a conventional optical microscope. Due to this diffraction limit, we cannot image the nanostructure by way of propagating light. However, metal structures such as a metal tip and antenna can confine fields to the subwavelength scale. Due to the capability to confine the electromagnetic field within subwavelength dimensions, SPP-based microscopes whose resolution can beat the diffraction limit have been emerging intensively [63].

2.2. Magnetic surface waves, e.g. magnetic plasmons (note: require negative permeability of one of the media)

Just as interfaces between metals and dielectrics support the propagation of surface plasmon polaritons, an interface between media with positive and negative permeabilities can support a magnetic equivalent of plasmons, called *magnetic plasmon* (MP). Note that MP is different from *surface magnetoplasmons* on gyrotropic media, which will be discussed later. Unlike negative permittivity, which can be easily given by metals, it is harder to realize negative permeability by naturally-occuring materials. Therefore, magnetic plasmons have been investigated in the context of negative index materials (NIMs) that possess simultaneously a negative permittivity and permeability, also termed double negative (DNG) materials [64, 65]. In such media, wavevector **k**, the electric and magnetic fields **E** and **H** form the left-handed triad rather than the typical right-handed triad in conventional materials. Therefore, they are also called left-handed materials (LHMs) as opposed to right-handed materials (RHMs), that is, conventional dielectrics with both positive permittivities and permeabilities. These unusual media were predicted by Veselago, who reported on the negative refraction of a light wave in such media in 1968 [66].

The origin of negative permeability is the resonance of an inductive element originating from the metal line with an electric current flow and a capacitive element, which occurs when electric charges are separated between metallic components of the LHM [27, 67]. At the resonance, the effective permeability, which is the net permeability of the whole periodic structure, can be negative in a certain frequency range [27]. In order to realize the resonance, a metallic line with an electric current for inductance and two pieces of metal close to each other for capacitive coupling are required. LHMs for the microwave regime were presented by split ring resonators composed of two concentric metal rings with different diameters and metal wires. Most of the early stage LHMs were made for the microwave and THz regions due to technical difficulties in the fabrication of such intricate structures. However, LHMs for the visible and near infrared regions were also demonstrated [27].

The normalized propagation constant (wavenumber) of a MP at the interface between a LHM and a RHM is given by [5]

$$N_{\mathrm{MP}} = k_{\mathrm{MP}}/k_0 = [\mu_r\mu_l(\varepsilon_r\mu_l - \varepsilon_l\mu_r)/(\mu_l^2 - \mu_r^2)]^{1/2}, \qquad (4)$$

where ε_r and μ_r, and ε_l and μ_l are the permittivity and permeability of the right-handed and left-handed materials, respectively. When the right-handed material is air ($\varepsilon_r = \mu_r = 1$), equation (4) is reduced to

$$N_{\mathrm{MP}} = k_{\mathrm{MP}}/k_0 = [\mu_l(\mu_l - \varepsilon_l)/(\mu_l^2 - 1)]^{1/2}. \qquad (5)$$

Depending on the material parameters, either TE- or TM-polarized surface waves can be supported at the interfaces between LHMs and RHMs as shown in figure 3. The TM mode resembles a surface plasmon polariton since it is caused by the negative permittivity of one medium in contact (see figure 3(b)). On the other hand, the TE mode, e.g. magnetic plasmon with the electric field parallel to the interface, originates from the negative permeability of the materials in contact (see figure 3(c)). Compared with the negative permittivity-based SPPs, the study of MPs has been not widely conducted except for some theoretical works [68–74]. This is probably due to the technical difficulties of fabricating negative permeability materials and the scarce number of naturally occurring materials available with negative permeability in the frequency range of interest. Apart from the theoretical works, experimental observation of MPs excited in the Otto configuration was reported in the microwave regime [5]. Localized magnetic plasmons in microwaves were also observed [75]. Furthermore, MPs for near-infrared wavelengths supported by the network of Au nanoparticles were studied [76, 77]. Paniagua-Dominquez *et al* studied scattering from a rough surface of LHM [78]. They showed that for $\varepsilon < 0$ and $\mu > 0$ the TM-polarized surface plasmon is responsible for the enhanced scattering, and for $\varepsilon > 0$ and $\mu < 0$ the TE-polarized magnetic plasmon is responsible for the

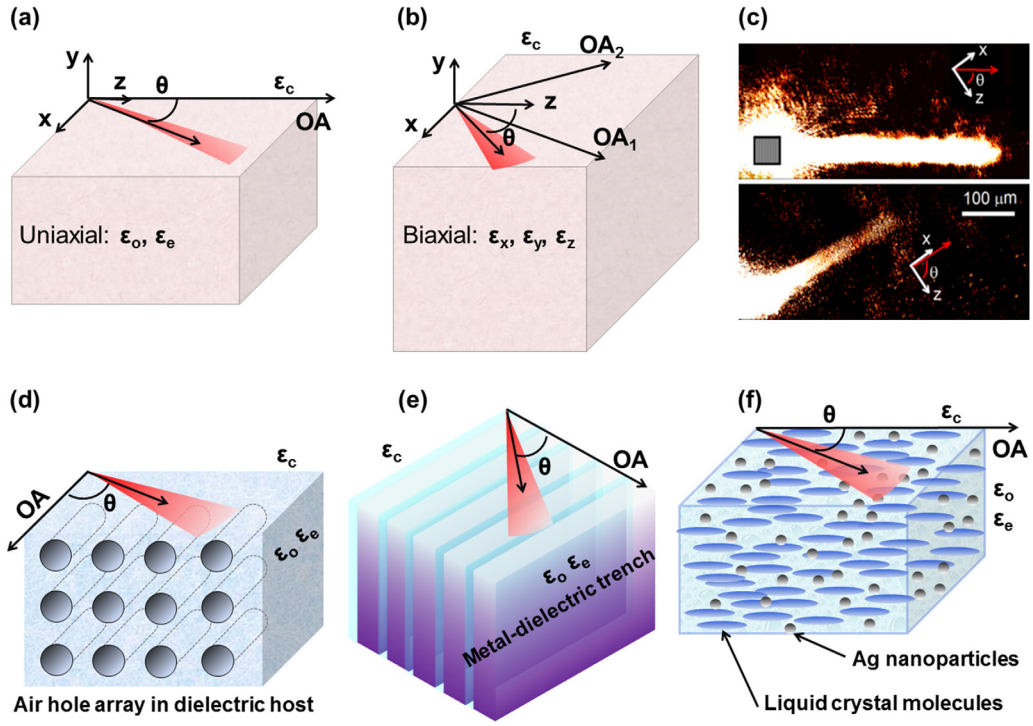

Figure 4. Surface waves on linear anisotropic media. (a) Dyakonov surface waves on semi-infinite uniaxial materials and (b) biaxial materials. The optical axes (OA) are in the plane of the interface. The surface waves propagate at a certain angle from the *x*-axis. (c) Direct observation of Dyakonov surface waves on biaxial material with a nanofilm, showing that a small change in the refractive index steers the propagation of the surface waves significantly [85]. Dyakonov surface waves on metamaterials of (d) air hole array in high refractive index dielectric matrix [87], (e) trench structures of dielectric and metal layers [88], and (f) Ag nanoparticles' dispersed liquid crystals [89]. For (d) and (e) the pitch of the structures is assumed to be sufficiently small compared with the operating wavelengths so that the effective media approximation holds. Reprinted by permission from Macmillan Publishers Ltd: Nature nanotechnology [85], Copyright 2014.

enhanced scattering. In fact, they showed that when $|\varepsilon| = |\mu|$ both cases of enhanced scattering occur for the same angle of incidence with the opposite polarization.

It is not only metamaterials with metallic components ($\varepsilon < 0$) that have effective permeability $\mu_{\text{eff}} > 0$, but also all-dielectric metamaterials made of dielectric components with large permittivity can generate $\varepsilon < 0$ due to the Mie resonances thus currently gaining attention [28]. A localized magnetic plasmon was theoretically shown to exist [79] when dielectric structures exhibit $\mu_{\text{eff}} < 0$ as opposed to a LHM with lossy metallic components. To date, propagating magnetic plasmons supported on dielectric metamaterials with negative permeability have not been observed. However, it may be advantageous for the microwave and THz regimes, where large permittivity materials are more available than those at optical frequencies.

2.3. Dyakonov surface waves (note: require linear anisotropy of one of the media)

A unique directional surface wave supported at a plane interface of two transparent media with at least one of them being linear anisotropic was predicted by Dyakonov in the late 1980s [6]. The dispersion of Dyakonov surface waves supported at the interface between isotropic and uniaxial materials with the optical axis in the plane of the interface is [6]

$$(\Gamma_c + \Gamma_e)(\Gamma_c + \Gamma_o)(\varepsilon_c\Gamma_o + \varepsilon_o\Gamma_e) = (\varepsilon_e - \varepsilon_c)(\varepsilon_c - \varepsilon_o)\Gamma_o, \tag{6}$$

where $\Gamma_c = (N^2 - \varepsilon_c)^{1/2}$, $\Gamma_o = (N^2 - \varepsilon_o)^{1/2}$, $\Gamma_e = [(N^2(\sin^2\theta + \varepsilon_e/\varepsilon_o \cos^2\theta) - \varepsilon_e)]^{1/2}$, N is the normalized wavenumber of SW, θ is the angle from the optical axis, ε_o and ε_e are the ordinary and extraordinary permittivities of the uniaxial anisotropic material, respectively, and ε_c is the permittivity of the isotropic material. The condition for the existence of Dyakonov surface waves is

$$\varepsilon_o < \varepsilon_c < \varepsilon_e. \tag{7}$$

In the case of the biaxial crystal isotropic medium interface, the condition is [80]

$$\varepsilon_x < \varepsilon_y < \varepsilon_c < \varepsilon_z, \tag{8}$$

where $\varepsilon_z > \varepsilon_y > \varepsilon_x$ are the principal values of the permittivity tensor of the biaxial crystal along the corresponding axis. Dyakonov surface waves exist on a surface of a biaxial material when its permittivity tensor $\hat{\varepsilon}$ is oriented in such way that both optical axes are in the plane of the interface as illustrated in figure 4(b). The features of the Dyakonov SWs excited in these geometries are summarized in the following four points:

(i) Dyakonov SWs propagate along the interfaces of transparent anisotropic materials, and therefore suffer little or no absorption.
(ii) Dyakonov SWs are highly directional, so that propagation is possible only in a narrow angular range with certain orientation relative to the optical axis as depicted in figures 4(a) and (b).

(iii) Dyakonov SWs are hybrid polarized waves, that is, they have simultaneously both TE- and TM-field components. Usually the TE character is dominant for a small birefringence [6].
(iv) The angular existence domain increases with the normalized birefringence, but besides this also depends on the permittivity of the cover isotropic media [6].

Since the initial theoretical prediction, there have been numerous theoretical works on various configurations and layouts supporting Dyakonov SWs [81]. However, the experiment was eventually realized only 20 years after the first publication. The first Dyakonov surface waves were demonstrated on a biaxial crystal (potassium titanyl phosphate or KTP) interface [82]. Later, following the theoretical prediction by Torner and co-workers [83, 84], where they envisaged the special nanosheet geometry for sensing and nanoguiding applications, such nano-sheet geometry was realized with lithium triborate (LBO) [85, 86]. In particular, the effective steering of directional Dyakonov waves by a small change of the dielectric environment was reported. The nanosheet waveguide structures are composed of either a positive uniaxial or biaxial substrate, an ultra-thin dielectric film (usually much thinner than the considered wavelength), and a semi-infinite isotropic cladding. The refractive indices of the isotropic medium and the birefringent substrate are chosen to satisfy the existence condition for Dyakonov SWs, equations (7) and (8). The permittivity of the dielectric nanosheets, ε_f, is chosen to be larger than those of other layers. In such a setting, guided modes preserve the principle feature of the Dyakonov SWs: directivity, having meanwhile a wider angular domain, improved localization and relaxed existence condition. The angular existence domain increases with the thickness of the film. In the limit where the thickness of the nanosheet becomes null, the guided mode transforms into the Dyakonov SW. In the LBO-based system with alumina nanosheets of 10 to 20 nm thicknesses, steering of guided modes by over 30 degrees in the propagation direction is possible. As demonstrated, the relevant change of the refractive index was as small as 0.015 RIU. Such numbers lead to the sensitivity $S = 5\times10^{-4}$ RIU/degree as shown in figure 4(c) [85]. This work also suggests that the refractive index of the environment in the vicinity of the interface is encoded in the direction of propagation and thus can be unambiguously detected, which may lead to the unique detection method. Moreover, the observed propagation length of the SWs was 200 to over 300 μm, depending on the propagation direction, thus also providing another detection/sensing characteristic.

Besides the isotropic-uniaxial and isotropic-biaxial interfaces, other possible combinations of media at the interfaces have been investigated too: the interface between two identical uniaxial media with crossed optical axes [90, 91], and interfaces between biaxial crystals [92, 93]. A review of the early stage research of Dyakonov surface waves (until 2008) can be found elsewhere [81]. Some later theoretical advances on the subject include the resonant transmission via Dyakonov surface waves [94] and coupling between Dyakonov SWs and plasmons on a metamaterial [95]. As for the tool to control the directivity of Dyakonov SWs, the Pockels effect was proposed in [96].

One of the greatest challenges in the exploitation of Dyakonov SWs which hindered the experimental demonstration of the phenomenon is the weak anisotropy of the natural birefringent media [81]. It results in a narrow propagation cone, typically less than one degree and extreme conditions for the waves' excitation. Moreover, in general, Dyakonov SWs are weakly localized. Here is the quest for metamaterials, which are expected to bring a high anisotropy and address these challenges comprehensively. Various metamaterial structures have been proposed as illustrated in figures 4(d)–(f). The interface between an isotropic LHM and a dielectric uniaxial medium was studied by Crasovan *et al* [97]. All-dielectric metamaterials made of air hole arrays in dielectric host media with a deep subwavelength pitch were proposed by Artigas *et al* [87]. In this work they showed that the anisotropy can be designed by the volume fraction of the air holes in the dielectric matrix and, therefore, the properties of Dyakonov SWs in terms of a wider propagation cone and level of localization can be improved. There are several studies showing that the inclusion of metallic components in periodic metamaterial structures significantly increases the effective anisotropy, enhancing localization and the angular existence domain of Dyakonov SWs. For instance, the trench structures made of vertical metal-dielectric multi-layers exhibit a large anisotropy and support Dyakonov SWs with several degrees of the angular existence domain [88, 98], which is considered to be reasonable for facile excitation. Moreover, the trench metal-dielectric metamaterials can exhibit hyperbolic dispersion in a range of wavelengths, where other types of surface waves, such as Dyakonov plasmons exist [88]. Metal nanoparticles dispersed in a liquid crystal provide highly anisotropic metamaterial structures, which were proposed for supporting Dyakonov SWs in the visible domain [89]. The anisotropy of such metamaterials can be controlled by the volume fraction of the nanoparticles, and furthermore their anisotropy in a liquid crystal-based system can be tuned by applying voltage, showing the potential of Dyakonov SWs for voltage-controled switching devices.

2.4. Dyakonov plasmons—Surface waves at the interfaces of hyperbolic metamaterials (note: require indefinite anisotropy of one of the media) and other hybrid states

Recently, hyperbolic metamaterials (HMMs) or indefinite media have gained attention due to their unique dispersion properties. Namely, the simultaneous presence of negative and positive components in the permittivity tensor provides extreme anisotropy and generates hyperbolic dispersion in the reciprocal space [20, 21, 99–101]. In particular, the hyperbolic isofrequency contours, unlimited in theory in the k-space, support very large wavevectors for light propagating in such media. Hyperbolic metamaterials are categorized into two types, depending on the sign of the permittivity tensor. Type I has $\varepsilon_o > 0$ and $\varepsilon_e < 0$, and Type II has $\varepsilon_o < 0$ and $\varepsilon_e > 0$ [102]. A special type of SWs are supported at the interface between dielectric with positive permittivity and type II

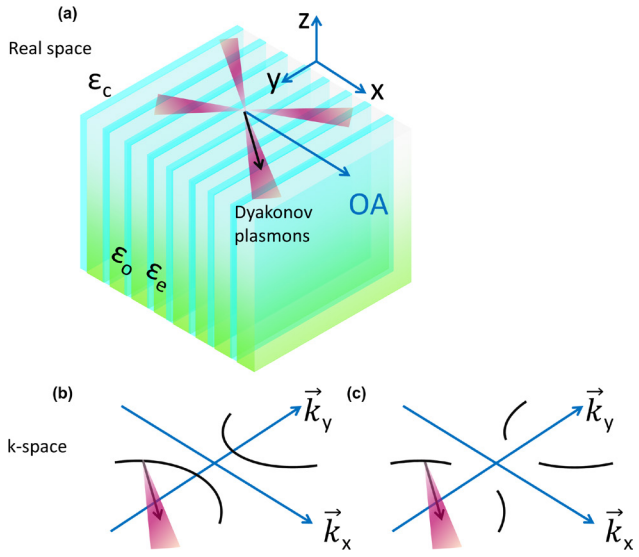

Figure 5. Directional propagation of Dyakonov plasmons. (a) Illustration of DPs on hyperbolic metamaterials (HMMs) in vertical metal-dielectric structures in the real space and corresponding (b) full and (c) partial hyperbolic dispersion in the k-space. For the long wavelength limit, the HMMs can be characterized by effective ordinary and extraordinary permittivities, ε_o and ε_e, respectively. The isotropic medium on HMM has permittivity ε_c.

HMMs. Such surface waves are called *Dyakonov plasmons* (DPs), being considered as a combination of Type 1 (requiring negative permittivity) and Type 3 (requiring linear anisotropy) surface waves. Importantly, these combined surface waves carry the traits of both primitive types of surface waves: high localization of SPPs (Type 1 SW) and directionality of Dyakonov SWs (Type 3 SW).

The features of DPs can be summarized as follows:

(i) DPs are directional SWs.
(ii) DPs have high localization due to the presence of high-k waves.
(iii) The level of localization can be controlled for the fixed wavelength by exciting different wavevectors, i.e. by the direction of propagation. In other words, there is high potential for tuning and control of the tail of the evanescent fields in both isotropic and/or HMM layers.
(iv) DPs are sensitive to the change of permittivity either of the isotropic layer, or of the HMM.
(v) Emission from a quantum light source placed on the surface of a HMM can be directional via coupling to Dyakonov plasmons [20, 21].

Assuming $\varepsilon_o < 0$ and $\varepsilon_e > 0$ (Type II HMM), there are two types of Dyakonov plasmons according to the permittivity relations. If

$$0 < \varepsilon_c < |\varepsilon_o|\varepsilon_e/|\varepsilon_e - \varepsilon_o|, \tag{9}$$

DPs have full hyperbolic dispersion (see figure 5(b)), and if

$$|\varepsilon_o|\varepsilon_e/|\varepsilon_e - \varepsilon_o| < \varepsilon_c < |\varepsilon_o|, \tag{10}$$

DPs have partial hyperbolic dispersion (see figures 5(c) and 6(a)) [88]. To illustrate the difference between the Dyakonov plasmon in the case of equation (9) and (10) and Dyakonov surface waves satisfying equation (7), as well as surface plasmon polaritions with equation (1), we show dispersion and field profiles in figure 6. Dyakonov plasmons on HMMs generally exhibit a wider allowed angle of propagation, larger wavevectors, and therefore a higher degree of localization at the interface than Dyakonov surface waves on a dielectric metamaterial ($\varepsilon_o = 2, \varepsilon_e = 10$, and $\varepsilon_c = 5$) as shown in figure 6. Both Dyakonov plasmons and Dyakonov surface waves are hybrid-polarized waves with both inseparable TE and TM fields components while a surface plasmon polariton is a pure TM-polarized wave as shown in figures 6(b)–(d).

In order to realize a macroscopic-sized metamaterial with Type II hyperbolic dispersion shown in figure 5, metal-dielectric vertical trench structures were proposed and analyzed [20, 21, 99, 101, 103]. The homogenization of such multi-layer systems can be fulfilled through the effective media approximation provided that the condition that the thicknesses of the layers are sufficiently small compared with the operating wavelengths is satisfied. The effective ordinary and extraordinary permittivities are then given by

$$\varepsilon_o = f_m\varepsilon_m + (1 - f_m)\varepsilon_d, \varepsilon_e = (f_m/\varepsilon_m + (1 - f_m)/\varepsilon_d)^{-1} \tag{11}$$

where ε_d and d_d are the permittivity and thickness of the dielectric layers and ε_m and d_m are those of the metal ones. f_m is the volume fraction of the metal layer, $f_m = d_m/(d_d + d_m)$. Note that equation (11) is valid only for wavevector $k_{//}$ which is parallel to the interface, and for very large values of $k_{//}$ dispersion starts to deviate from that predicted by the effective medium model [104]. The challenge in realization of such a metamaterial structure lies in the reproducible fabrication of deep subwavelength trenches extended over a large area as shown in figure 5.

SWs on biaxial HMMs have been considered recently [105]. Besides the permittivity-based HMMs, SWs on HMMs with a hyperbolic permeability tensor were studied in [106]. The existence conditions of SWs, including those with hyperbolic dispersion in terms of the permittivity and permeability, were derived. At the interface between the isotropic metal and uniaxial dielectric there are various kinds of SWs, some of which possess hyperbolic dispersion [107]. Following the directional propagation of SWs on the surface of a hyperbolic metamaterial, emission from a quantum light source can be directional as well since light emitted from the quantum emitter on the HMM is more efficiently coupled to the directional surface waves [20, 21]. This suggests the possibility of making a directional collective quantum emitter or single photon light source when emitters are placed on the surface of the HMM that supports the directional SWs.

2.5. Nonreciprocal surface waves on optically active or gyrotropic materials (note: require circular anisotropy of one of the media)

A *bianisotropic* material gives a linear optical response and exhibits magnetoelectric coupling, that is a magnetic field generates electric polarization in the medium, and vice versa. The optical response of the bianisotropic material can be described by

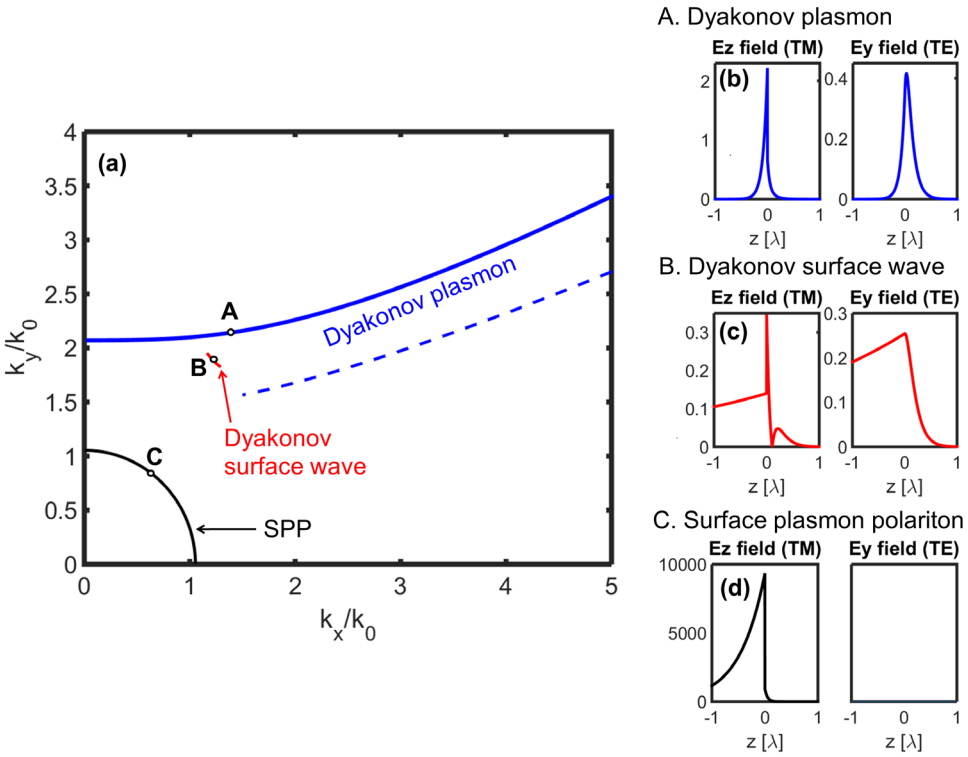

Figure 6. Difference between Dyakonov plasmons and Dyakonov surface waves. (a) k-space dispersion of Dyakonov plasmons with $\varepsilon_o = -10$, $\varepsilon_e = 2$, and $\varepsilon_c = 1$ obeying equation (9) (blue dashed), $\varepsilon_c = 3$, equation (10) (blue solid), and Dyakonov surface waves with $\varepsilon_o = 2$, $\varepsilon_e = 10$, $\varepsilon_c = 5$, equation (7) (red solid) and surface plasmon polariton on air-isotropic metal interface with $\varepsilon_o = \varepsilon_e = -10$ and $\varepsilon_c = 1$. Field profile (norm) of (b) Dyakonov plasmon, (c) Dyakonov surface wave (d) surface plasmon polarition at points A, B and C in (a), respectively. Isotropic medium with ε_c is at $z < 0$ and HMM or metal characterized by ε_o and ε_e is located at $z > 0$. Note that the x, y, z coordinates are the same as in figure 5(a).

$$\mathbf{D} = \hat{\varepsilon}\mathbf{E} + \hat{\xi}\mathbf{H}, \mathbf{B} = \hat{\mu}\mathbf{H} + \hat{\zeta}\mathbf{E}, \tag{12}$$

where $\hat{\varepsilon}, \hat{\mu}, \hat{\xi}$ and $\hat{\zeta}$ in general are tensors. *Chiral* or *optically active* media are a special case of bianisotropic media, where the four tensors in equation (12) become scalar parameters,

$$\mathbf{D} = \varepsilon\mathbf{E} + \mathrm{i}\xi\mathbf{H}, \mathbf{B} = \mu\mathbf{H} + \mathrm{i}\zeta\mathbf{E}, \tag{13}$$

where ζ and ξ describe the chiral properties of the medium [108]. Chiral media are circularly birefringent in contrast to linear birefringent media that support Dyakonov SWs (see the previous subsections). In such chiral materials, the polarization plane of a transmitted plane wave is rotated relative to the incident one. This phenomenon is also termed optical activity. Waves with right- and left-circular polarizations propagate with different speeds, or in other words, experience different refractive indices. Examples of chiral media are: sugar solutions, proteins, lipids, nucleic acids, amino acids, DNA, vitamins, hormones, and cholesteric liquid crystals with helical-like molecular structures.

The first theoretical studies of SWs at the boundary of isotropic-chiral materials were reported by Pattanayak and Birman in early 1980s [109]. For optical wavelengths, numerical analysis for the Otto-configuration of the prism-vacuum-chiral structure was conducted with quarts and $NaClO_3$, and it was shown that the SWs are elliptic-polarized waves [110]. Later, microwave surface waves were investigated both theoretically and experimentally [111].

Some isotropic materials generate optical activity being exposed for a constant magnetic field, which breaks their isotropy—the so-called magneto-optic or Faraday effect as illustrated in figure 8(a). Such a medium is a gyrotropic material in which the propagating wave's polarization is rotated as the wave passes through. There are two kinds of gyrotropic materials, namely, gyroelectric and gyromagnetic, depending on their gyrotropic contribution in the permittivity or permeability. For example, for monochromatic waves the dielectric tensor of a gyroelectric material is expressed in the Hermitian form

$$\hat{\varepsilon} = \begin{bmatrix} \varepsilon_1 & \mathrm{i}\varepsilon_2 & 0 \\ -\mathrm{i}\varepsilon_2 & \varepsilon_1 & 0 \\ 0 & 0 & \varepsilon_3 \end{bmatrix}, \mathbf{D} = \hat{\varepsilon}\mathbf{E} \tag{14}$$

where the off-diagonal components ε_2 depend on the material and strength of the magnetic field. Similarly, gyromagnetic materials are characterized by the Hermitian permeability tensor in the form

$$\hat{\mu} = \begin{bmatrix} \mu_1 & \mathrm{i}\mu_2 & 0 \\ -\mathrm{i}\mu_2 & \mu_1 & 0 \\ 0 & 0 & \mu_3 \end{bmatrix}, \mathbf{B} = \hat{\mu}\mathbf{H} \tag{15}$$

where the expressions of the components are different depending on whether the material is ferromagnetic or antiferromagnetic. When there is no magnetic field applied the off-diagonal components are nullified for antiferromagnets, while those of ferromagnets take non-zero values. There are two different

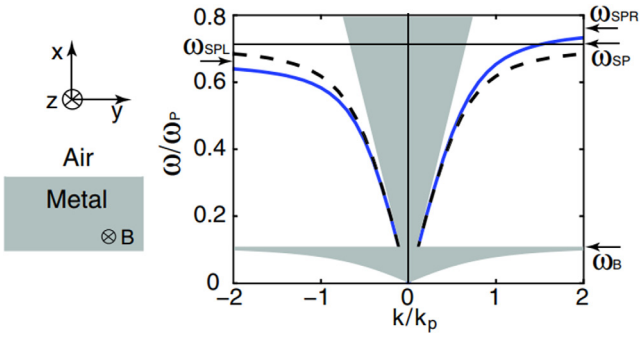

Figure 7. One-way propagation of non-reciprocal surface waves supported at the interface of air and free-electron metal subjects to an externally applied magnetic field along the z direction. Dispersion relations of surface plasmons at metal–air interfaces in the presence (solid blue line) or absence (dashed black line) of an externally applied static magnetic field. The gray regions represent extended modes in air and metal. Reprinted figure with permission from [114], Copyright 2008 by the American Physical Society.

classes of SWs on gyrotropic materials, surface magnetoplasmons on gyroelectric media characterized by equation (14) and surface magnetostatic spin waves on gyromagnetic materials, characterized by equation (15) [7].

Nonreciprocal plasmons or *surface magnetoplasmons* are supported at the interface between the isotropic dielectric and material with a gyrotropic permittivity tensor induced by a magnetic field and characterized by equation (14). Surface magnetoplasmons were theoretically investigated in 1972 for doped semiconductors such as GaAS and InSb in the frequency range of 100–500 GHz [112, 113]. SWs were studied on the air–doped semiconductors interface, where a constant magnetic field is applied parallel to the plane of the interface but perpendicular to the direction of the SW propagation. The most remarkable and unique characteristic of these SWs is their non-reciprocity in the dispersion as well as the angular dependence of propagation in the plane interface. That is, although the SW can propagate in one direction with a positive wave vector, it cannot propagate in the opposite direction. In other cases the SWs are allowed to propagate but with a wavevector that is different from the propagation in the forward direction. Typical dispersion of such non-reciprocal surface waves is shown in figure 7 [114]. In 1984, the non-reciprocal behavior of the SWs on gyrotropic media was experimentally observed for a n-type InSb semiconductor [115], showing that the amplitude of the external magnetic field influences the wavevector of SWs.

The other feature of surface magnetoplasmons is that the propagation of the surface waves can be controlled or tuned by an applied magnetic field [116–118], and the propagation of SWs can be made unidirectional or its effective refractive indices are tuned for different directions. Applications of such magneto-optic plasmon devices include optical switching and modulation by the external magnetic field, and optical isolators for SWs. These were theoretically analyzed for the interface between the gyrotropic metal and dielectric photonic crystal by Fan *et al* [114]. Moreover, edge states of a 2D gyromagnetic photonic crystal were theoretically shown to exist by Soljačić [23]. Temnov *et al* demonstrated the phase control and modulation of gap plasmons by a DC magnetic field, where plasmon modes were supported on a metal(Au)-ferromagnet(Co)-metal(Au) structure for near-infrared wavelengths [119]. Modulation of the optical properties of SWs using magnetization control by relatively weak magnetic fields suggests application of such systems as optical switches.

Furs and Barkovsky theoretically investigated the SW at the boundary of isotropic and gyrotropic media, and showed that there is a threshold for the applied external magnetic field to support SWs [120]. They also studied the existence conditions for SWs on the interface between the gyromagnetic [121] and gyroelectric media with identical permittivity and permeability tensors [122]. SWs were analyzed not only for homogeneous gyrotropic media but also for multilayers of alternating gyrotropic and non-magnetic materials [123], as shown in figure 8(b). In this case, the magnetic stack of ferrimagnetic layers (gyrotropic) is effectively a semi-infinite gyrotropic metamaterial. Moreover, SWs on the lateral side of the magnetic stack (or one-dimensional photonic crystal) as illustrated in figure 8(c) also exist [124]. The authors of the latter reference showed that for the SWs propagation there is a threshold of applied magnetic field, and the angular existence domain depends on the magnetic field. The combination of gytropic media and LHMs was also considered as reported in [125].

3. Surface waves on the interfaces of photonic bandgap structures

Photonic crystals (PhCs) are materials with periodically modulated refractive indices. The unit cell of a PhC could be composed of different materials such as dielectrics, semiconductors, or metals [126]. Periodic modulation of the refractive index in space results in the appearance of photonic bandgaps (PBGs) in analogy with electron bandgaps in semiconductors [30]. A PBG represents a range of frequencies forbidden for the propagation of photons inside a photonic crystal. The forbidden frequencies range depends on the momentum of the photons and waves polarization. The frequency range forbidden for all propagation directions and polarizations is called a complete photonic bandgap. Note that unlike metamaterials, for which periodicity is much smaller than the wavelength under consideration, the periodicity of photonic crystals is comparable to the wavelength, typically being in the range of half to a quarter of the wavelengths. The refractive index of PhCs can be modulated in one, two, or all three dimensions. Consequently, PhCs are called one- (1D), two- (2D), and three-dimensional (3D). 1D PhCs are also known as distributed Bragg reflectors (DBR) or multilayer structures. In this section we discuss surface waves supported by the interfaces of such periodic structures [127, 128].

3.1. Optical Tamm states and Bloch surface waves on truncated photonic crystal (note: require periodic permittivity of one of the media)

Originally, Tamm states are electronic states localized at the terminations of a periodic lattice, e.g. at the surface of

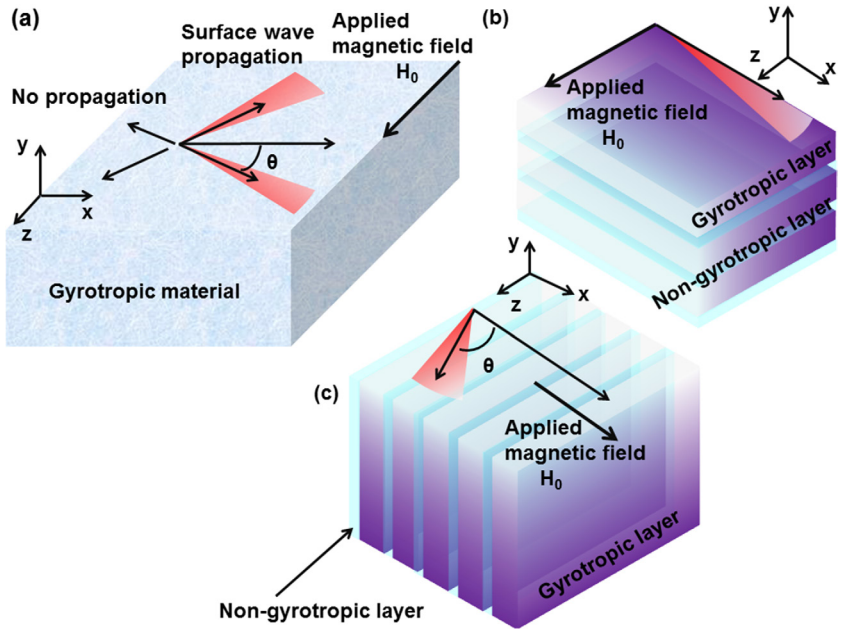

Figure 8. Surface waves on gyrotropic media. (a) Surface waves on semi-infinite gyrotropic material. The magnetic field is applied parallel to the interface along the *z*-axis. The surface waves propagate at a certain angle from the *x*-axis. A schematic illustration of lateral antiferromagnetic and nonmagnetic multilayers stack where (b) surface waves propagate on the top layer and (c) at the edge of the stack.

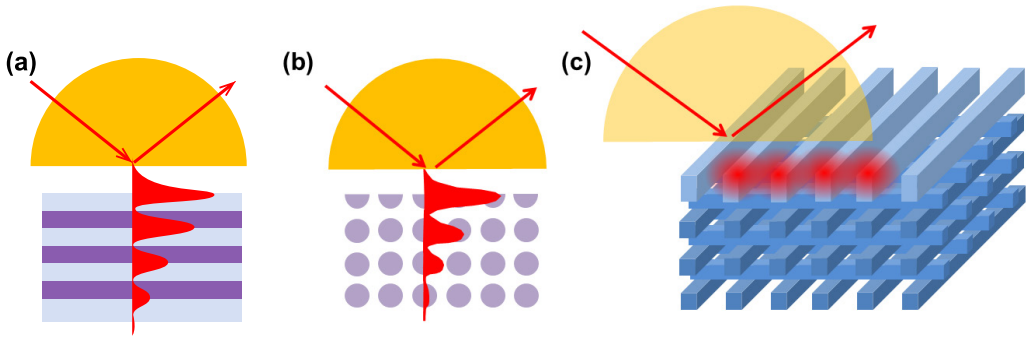

Figure 9. Surface waves on truncated photonic crsytals. (a) 1D photonic crystal composed of bilayers of two dielectrics. (b) 2D photonic crystal made of dielectric cylinders. (c) 3D photonic crystal, so-called woodpile structure, composed of dielectric rods. The terminating layer may have a thickness that is different from the other layers. In many cases, surface waves are excited by the Otto-Kretchmann configuration.

the material with periodic potential [129]. First they were observed on the surface of a semiconductor superlattice [130]. An optical equivalent of electronic Tamm states occurs at the interface of the terminated photonic crystal structures (see figure 9(a)) on frequencies within the PBG range. In optics such states are often referred to as *Bloch surface waves* [131–133]. However, in the absence of periodicity in the direction of propagation such a notion is dubious. Drawing a parallel with solid state physics we prefer the term *optical Tamm states*. Alternatively they can be referred to as surface states, as in [128]. We will apply the term Bloch surface waves only in the cases if periodicity exists in the interface of the SWs confinement [103, 134, 135].

In the case of one-dimensional (1D) PhCs, or in other words, periodic stacks of dielectric layers as illustrated in figure 9(a), surface bounded modes were first predicted in the 1960s [136] and observed for the GaAs and AlGaAs multilayer in [8]. An experimental work showed that variations in the thickness results in a change of the wavelength and in-plane wavevector of the SWs [137]. This property of the wavelength shift was proposed for sensing applications [138]. The typical field profile of optical Tamm states on a 1D PhC is illustrated in figure 9(a). The field maxima are located at the vicinity of the PhC structure and decay with an exponential envelope in the PhC, while the field also decays exponentially into the ambient medium, i.e. air. One of the advantages of optical Tamm states is that they are supported by transparent dielectric structures with a high degree of localization. The Tamm SWs were analyzed for waveguide structures and resonators on top of 1D PhCs [132]. The Tamm SWs at the interface of metal-dielectric PhC were considered in [139–142]. It was shown that in the vicinity of the plasma frequency properties of the Tamm SWs become similar to the properties of SPPs. The anisotropy of plasma frequency in metal layers could lift the degeneracy of plasma oscillations and open a series of PBGs [143]. This results in the appearance of *Tamm-Langmuir SWs* with singular density of states [104, 144].

SWs on the surface of two-dimensional (2D) PhCs are excited on a microwave frequency (tens of GHz) by prism coupling [145, 146]. In this case, the PhC structure was made of dielectric rods with the last layer composed of half-cut dielectric rods as illustrated in figure 9(b). Note that in such a case the term 'Bloch surface wave' is consistent with the properties of the wave. The influence of the shape of the terminating layer was theoretically investigated for tuning the wavelength and wavevector of the SW on the PhC structures [138, 147], and experimentally verified. The shape and material of the terminating layer influence the directionality of the surface waves that can propagate forward or backward to the parallel wavevector of the Otto configuration [148]. SWs on 2D PhCs were observed for the mid-infrared wavelength on honeycomb structures that mimic graphene [149].

At the interface of three-dimensional (3D) PhCs, SWs were theoretically analyzed for a Yablonobite structure (see [150]) and observed for a woodpile structure, where a 3D periodic structure of semiconductor rods (GaAs) was constructed as shown in figure 9(c). The terminating layer at the interface with air has a slightly different height of dielectric rods. The surface waves are excited by the Otto configuration and the propagation distance was measured to be around 385 μm on the wavelength of 1.43 μm [151].

3.2. Dyakonov–Tamm waves

Dyakonov–Tamm waves (or states) are hybrid waves with a combination of Type 3 (Dyakonov surface waves on linear anisotropic media) and Type 5 (Optical Tamm states on systems with periodic permittivity). They are supported on the interface with anisotropic, in particular uniaxial, media whose anisotropy changes periodically along the direction perpendicular to the interface. As an example of such a structure, Lakhtakia and Polo Jr proposed the helical dielectric pillar structures as illustrated in figure 10(a) [1]. This structure is equivalent to the combination of anisotropic media and a periodic structure along the direction normal to the interface. When the helical pillar structure is attached to an isotropic medium, Dyakonov–Tamm states are supported between the isotropic and helical media. In the reported case with the helical pillars made of titanium dioxide (TiO_2), Dyakonov–Tamm waves were excited in the Otto-Kretschmann configuration [152] and also by the grating coupling scheme [153]. It turned out that the angular existence range of the surface wave is much wider (dozens of degrees) than that of a Dyakonov surface wave counterpart on natural anisotropic media (less than one degree). Apart from these studies, the combination of birefringent media and periodic structures for the purpose of forming an interface for SWs was theoretically investigated by Ciumac and colleagues [154]. They considered a positive uniaxial birefringent substrate with the optical axis in the plane of the interface and a dielectric multilayer composed of two different alternating dielectric layers. The refractive indices of the 1D photonic crystals, n_1 and n_2 satisfy the condition for a Dyakonov SW, namely,

$$n_o < n_1 < n_e \tag{16}$$

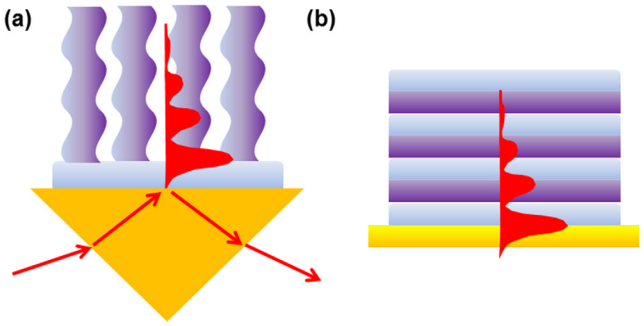

Figure 10. (a) Dyakonov–Tamm waves on helical dielectric metamaterials excited in the Kretschmann configuration with a coupling prism. (b) Tamm-plasmons on photonic crystals composed of dielectric layers of high and low refractive indices on a metal film.

and

$$n_o < n_2 < n_e. \tag{17}$$

As a result, hybrid surface modes are supported within a narrow angular existence domain.

3.3. Tamm plasmons

Tamm plasmons are the hybrid SWs (of Type 1 and Type 5 SWs) if a metal film cups a 1D PhC or a DBR that is the periodic arrangement of two different dielectric layers as shown in figure 10(b). These combined SWs were predicted by Kaliteevski *et al* [155]. This group also reported on the first experimental observation of Tamm plasmons formed at the interface between a metal layer (Au) and a dielectric Bragg reflector (GaAs/AlAs). Unlike conventional surface plasmons, Tamm plasmons can be both TE and TM-polarized modes and have an in-plane wave vector less than the wavevector of light in vacuum, which allows for free space optical excitation and out coupling without a prism [156].

Tamm plasmon modes have been investigated mostly for the development of light emitting devices such as lasers and diodes according to several advantages offered by the SWs. The localization of Tamm plasmons enable one to control and modify the radiation pattern of the laser by shaping the metallic layer on top of the DBR. This efficient coupling of the spontaneous emission into the Tamm mode helps to reduce the laser threshold. Since Tamm plasmon modes are supported on relatively simple multilayer structures, fabrication of the required structures is relatively easy. The metal layer itself can be used as an electrode for electric gating or carriers injection. Laser emission facilitated by Tamm plasmons is demonstrated for the active semiconductor DBR structure (30 periods of AlAs/AlGaAs layers) on a GaAs substrate coated with a metal thin film (Ag) [157]. Moreover, shaping the metal layer on the DBR brings additional control of the emission polarization [158]. Excitation of Tamm plasmon modes by the emission from quantum dots on top of a metal layer coating a dielectric DBR was also demonstrated [159]. Besides the lasing applications, refractive index sensing can also be enhanced by involving Tamm plasmons [160].

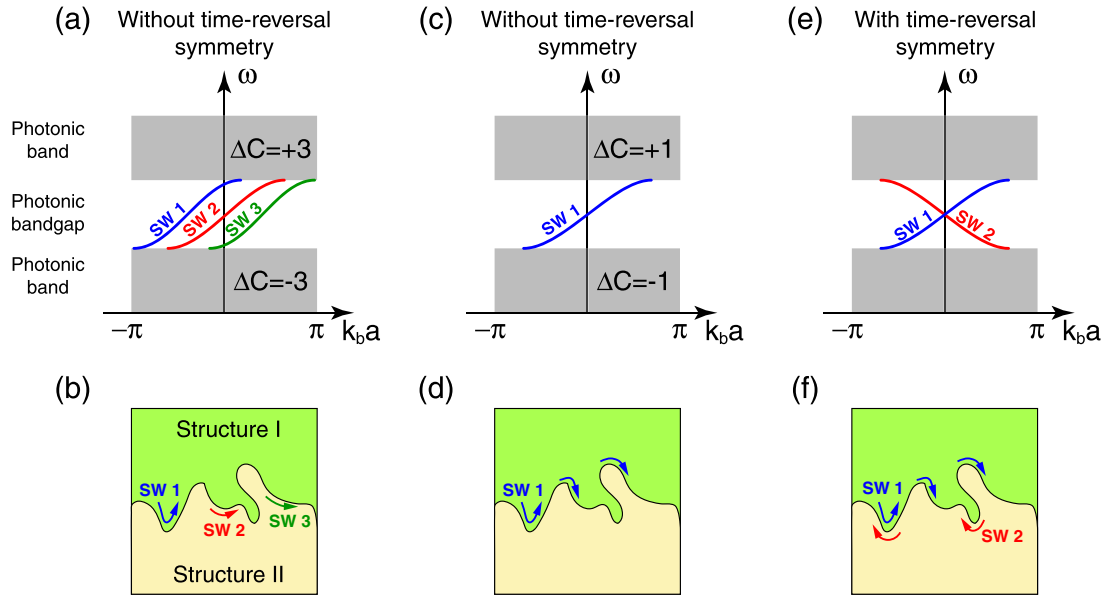

Figure 11. The photonic band diagram for the adjacent non-trivial photonic structures with ((a) and (c)) broken and (e) unbroken time-reversal symmetry. Here we suppose that both photonic structures have the same position and width of the PBG. ΔC is the difference between the Chern numbers for the photonic bands of the adjacent photonic structures *I* and *II*. The modulus of ΔC equals the number of the edge waves. Propagation of the edge waves in the case of ((b) and (d)) broken and (f) unbroken time-reversal symmetry.

3.4. Topological states

Topological photonics is a new and fast-growing branch of modern optics. It allows one to create photonics structures supporting unusual electromagnetic edge/surface waves insensitive to disorder and capable of propagating unidirectionally without scattering on obstacles and imperfections. This makes topological photonics very promising in a variety of applications, from sensors and slow light devices to couplers and photonic circuits immune to fabrication intolerances. The recent achievements of topological photonics are reviewed in [161–163].

The simplest object studied in topological photonics is a thin structure periodical in two dimensions made of metal or dielectric. For such a structure, it is more correct to use the term *edge waves* than *surface waves*. The topological properties of the photonic structures are usually understood as the topological properties of their photonic bands representing manifolds in the **k**-space. The key parameter characterizing the topological properties of the photonics bands is the Chern number *C* [163]. Usually, it is defined as an integral over the Berry curvature of the whole band. It equals an integer and plays the role of an additional degree of freedom along with momentum, frequency, polarization, and angular momentum. Structures with zero Chern numbers are called *topologically trivial* and structures with nonzero Chern numbers are correspondingly *topologically nontrivial*. All the structures considered above (metals, Bragg mirrors, dielectrics providing total internal reflections) are topologically trivial.

Topological edge waves appear at the interface of two photonic structures with overlapped PBGs and different Chern numbers. The number of topologically protected edge states is calculated as the difference between the Chern numbers of each photonic structure, while the sign of this difference indicates the propagation directions of the topological edge states (see figures 11(a)–(d)). The most robust topological insulators demand the breaking of the time-reversal symmetry. In this case, we completely suppress the unidirectional propagating modes and backscattering. The time-reversal symmetry can be broken in photonic crystals made of magneto-optical materials placed in a DC magnetic field. The unidirectional edge waves in the gyroelectric and gyromagnetic photonic structures were analyzed in [23, 164–166]. Another way to break the time-reversal symmetry is to use time-dependent modulations of the coupling constants between the resonators constituting a photonic crystal [167]. Since it is quite challenging to break the time-reversal symmetry at optical frequencies, alternative ideas to realize topologically nontrivial structures are reviewed in [162].

If time-reversal symmetry is not broken then for each edge wave there is a counterpropagating wave (see figures 11(e) and 11(f)). In spite of the fact that backscattering of edge/surface states is unavoidable in structures with time-reversal symmetry, it can be substantially suppressed, for example, via separation of the polarization of the counterpropagating edge waves [168]. This approach was experimentally confirmed with metallic and all-dielectric metasurfaces [169, 170] and metacrystals [171, 172]. Topologically protected surface waves can exist on the interface of 3D structures with topologically distinct properties. Recently, several designs of such a structure based on an all-dielectric platform [25], magneto-plasma [173], hyperbolic-gyromagnetic metamaterials [174], and ferrimagnetics [175] have been proposed.

4. Nonlinear surface waves

In this section, we discuss nonlinear SWs including nonlinear Dyakonov SWs at the interfaces between isotropic nonlinear materials whose permittivity depends on the intensity of light and linear uniaxial materials.

4.1. Surface solitons on nonlinear media

Interfaces between linear and nonlinear (NL) media are also known to support different types of SWs. *Surface solitons* [9] have been studied with the motivation to realize all-optical processing of information for computing, routing, and switching of information. The fundamental mechanism of SWs on NL media is that an intense optical beam changes the refractive index at the vicinity of the interface between nonlinear and linear media, making it higher, so that the light wave propagates through the self-induced high-index region. The investigation of SWs was conducted for Kerr type NL media extensively in 1980s and 1990s [9, 176–178]. The Kerr-type nonlinearity is characterized by quadratic dependence of the induced dielectric function on the electric field amplitude:

$$\varepsilon = \varepsilon_0 + \varepsilon_{\mathrm{NL}}|E|^2. \tag{18}$$

The Kerr type media can be categorized into two cases with a pure Kerr phenomenon where the refractive index of the media increases infinitely with the intensity of the field [9, 176, 177], and saturable Kerr nonlinearity, where the refractive index change saturates with a certain threshold value of the intensity [178]. The Kerr nonlinearity introduced in single layer of 1D periodic photonic structures could result in the appearance of *nonlinear Tamm waves*, which do not exist in the linear case [179, 180].

4.2. Nonlinear Dyakonov surface waves

Since the propagation direction of Dyakonov SWs is sensitive to the refractive indices of the media at the interface, steering of the surface waves by nonlinearity of an isotropic material is proposed by Torner *et al* [181]. The possibility of varying the refractive index by means of light intensity in nonlinear materials can be exploited to control the propagation of Dyakonov SWs. At the interface between nonlinear isotropic and linear birefringent materials in the linear limit, the existence requirement for the Dyakonov SW, expressed by equation (7), is satisfied. A Kerr-like nonlinearity characterized by equation (18) was assumed for the isotropic medium. TE-dominant nonlinear SWs were shown to exist outside the angular existence domain of the linear SWs. Depending on the particular orientation of the optical axis, the guided power of these nonlinear SWs varies with the effective refractive index of the modes. For a given material, one can tune the threshold power of the nonlinear Dyakonov SWs by modifying the orientation of the optic axis. Moreover, for certain propagation directions different from the optical axis, the threshold power of the nonlinear SW can be tuned by means of the refractive index of the isotropic medium. Later on, waveguide structures with a linear isotropic thin film inserted between the nonlinear isotropic medium and the birefringent medium were investigated, showing similar behavior as the single interface case [182]. These studies revealed another possibility to steer the directional surface waves by means of the nonlinear effect, different from voltage steering by the Pockels effect [96], polarization state steering [183], and spectral steering [99].

5. Surface waves on metasurfaces and natural 2D materials

5.1. General theory of 2D surface waves

In the previous sections we analyzed surface waves localized at the interfaces separating two bulk media. Here, we proceed with the analysis of surface waves localized at 2D materials. Such materials could be natural, such as graphene, silicene, and hexagonal boron nitride, or artificial like a *metasurface*. Metasurfaces are a two-dimensional analogue of bulk metamaterials. They represent a dense array (usually periodic) of subwavelength scatterers, which are often called meta-atoms. The term metasurface has been introduced recently, but such objects are fairly well-known in electromagnetism as impedance or frequency selective surfaces [184, 185]. Metasurfaces possess many properties of bulk metamaterials being, at the same time, much less lossy, cheaper in fabrication, fully compatible with planar technologies, and ready to be implanted in modern on-chip devices. They offer unprecedented control over phase, amplitude, polarization, propagation directions, and wavefront features of reflected and transmitted waves [186].

The deep subwavelength structure of metasurfaces allows one to describe them in terms of effective parameters. An isotropic, non-magnetic metasurface with a local electromagnetic response can be described by frequency-dependent scalar conductivity $\sigma(\omega)$ determining the relation between two-dimensional surface current $\mathbf{j}_{2\mathrm{D}}$ and electric field $\mathbf{E}$:

$$\mathbf{j}_{2\mathrm{D}} = \sigma(\omega)\mathbf{E}. \tag{19}$$

The same relation takes place, for example, for graphene or a dense array of isotropic non-magnetic meta-atoms. Two-dimensionality of the conductivity tensor implies that the polarizability of the metasurface in the normal direction is negligible. The field on the metasurface should meet the following boundary conditions:

$$[\mathbf{n}, \mathbf{H_2}] - [\mathbf{n}, \mathbf{H_1}] = \frac{4\pi}{c}\sigma(\omega, \mathbf{k})\mathbf{E} \tag{20}$$

$$[\mathbf{n}, \mathbf{E_2}] - [\mathbf{n}, \mathbf{E_1}] = 0. \tag{21}$$

Note that we use the Gaussian systems of units. Solution of Maxwell's equations in the form of a surface wave propagating along the metasurface gives the factorized dispersion equation:

$$\left(\frac{c\kappa}{\omega} - \frac{2\pi \mathrm{i}}{c}\sigma(\omega)\right) \times \left(\frac{\omega}{c\kappa} + \frac{2\pi \mathrm{i}}{c}\sigma(\omega)\right) = 0. \tag{22}$$

Here $\kappa^2 = k_z^2 - \omega^2/c^2$. This equation has two solutions. It can be shown straightforwardly from Maxwell's equations that these solutions correspond to the TE- and TM-plasmons [17, 187, 188]:

$$\mathrm{TE-plasmon}: \quad \mathrm{i}\sigma(\omega) = \frac{c^2\kappa}{2\pi\omega} \tag{23}$$

$$\mathrm{TM-plasmon}: \quad \mathrm{i}\sigma(\omega) = -\frac{\omega}{2\pi\kappa}. \tag{24}$$

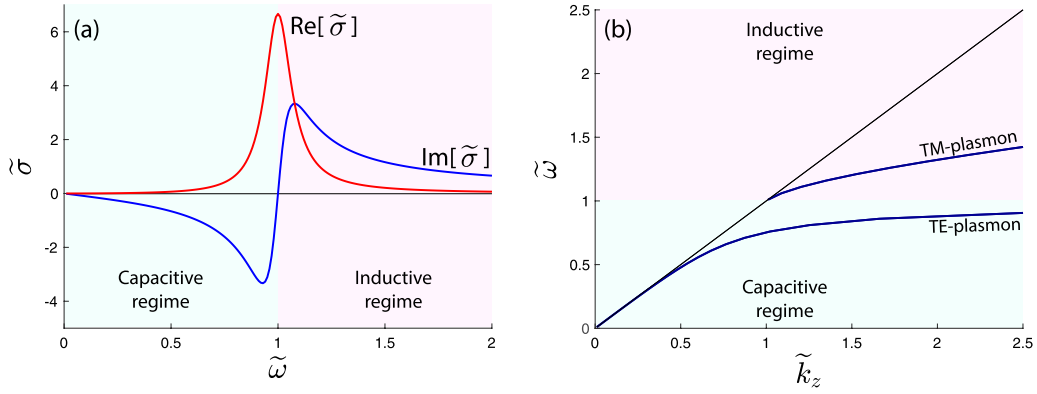

Figure 12. (a) Frequency dependence of the real and imaginary parts of conductivity. (b) Dispersion of TE- and TM-plasmons propagating along the resonant metasurface in the inductive and capacitive regimes. All graphics are plotted using the following dimensionless parameters: $\widetilde{\sigma} = 4\pi\sigma/c; \widetilde{\omega} = \omega/D; \widetilde{\gamma} = \gamma/D; \widetilde{k}_z = ck_z/D$. Resonant frequency $\widetilde{\Omega} = 1$ and damping factor $\widetilde{\gamma} = 0.15$.

One can see that TE-plasmon exists only if $\mathrm{Im}[\sigma(\omega)] < 0$ and TM-plasmon exists only if $\mathrm{Im}[\sigma(\omega)] > 0$. It is obvious that simultaneous propagation of both TE- and TM-plasmons is impossible.

The conductivity of a wide class of 2D materials could be described within the Drude-Lorentz approximation (see figure 12):

$$\sigma(\omega) = D\frac{\mathrm{i}c}{4\pi}\frac{\omega}{\omega^2 - \Omega^2 + \mathrm{i}\gamma\omega}. \tag{25}$$

Here D is a constant that depends on design, Ω is the resonant frequency of the meta-atom, and γ is the damping parameter. Therefore, at low frequencies $\omega \ll \Omega$ we have only a TE-plasmon with almost linear dispersion

$$k_z = \frac{\omega}{c} + \frac{\omega^2 D^2}{8\Omega^4}. \tag{26}$$

At high frequencies ($\omega \gg \Omega$) we have only a TM-plasmon with quadratic dispersion

$$k_z = 2\frac{\omega^2}{cD}. \tag{27}$$

The TE-plasmon can propagate at arbitrary low frequencies and have the maximal propagation frequency Ω at which $k_z \gg \Omega/c$. The TM-plasmon has a frequency cut-off Ω and it can propagate at arbitrary high frequencies. The dispersion of TE- and TM-plasmons on the metasurface described by the Drude-Lorentz response is shown in figure 12.

Experimentally, 2D TE- and TM-plasmons were observed in the radio-frequency range in high-impedance surface based antennas [189, 190] or two-dimensional metamaterial based transmission lines [191]. In two-dimensional metamaterials, it is possible to steer the surface waves due to the photonic spin Hall effect [183]. In the infrared and terahertz ranges, TE- and TM-plasmons can exist on graphene [17].

Recently, directional SWs have been predicted on a metasurface made of a subwavelength Ag grating [192]. They were experimentally observed as reported in [99]. For mid-infrared wavelengths some 2D materials, such as hexagonal boron nitride (hBN), function as hyperbolic materials due to a phonon resonance and support the phonon-polariton equivalent of Dyakonov plasmons [193], as well as other types of surface waves [38, 39].

5.2. Surface waves on an anisotropic metasurface

If a metasurface consists of meta-atoms with an anisotropic resonant response, its optical properties are described by the tensorial conductivity:

$$\hat{\sigma}(\omega) = \begin{pmatrix} \sigma_\perp & 0 \\ 0 & \sigma_\parallel \end{pmatrix} \tag{28}$$

$$\sigma_s(\omega) = D_s\frac{\mathrm{i}c}{4\pi}\frac{\omega}{\omega^2 - \Omega_s^2 + \mathrm{i}\gamma_s\omega}, \quad s = \perp, \parallel. \tag{29}$$

Such a metasurface can be realized as an array of graphene strips or anisotropic plasmonic nanoparticles (see figure 13(a)). In this case we have the following dispersion equation:

$$\left(\frac{c\kappa}{\omega} - \frac{2\pi\mathrm{i}}{c}\sigma_{yy}\right) \times \left(\frac{\omega}{c\kappa} + \frac{2\pi\mathrm{i}}{c}\sigma_{zz}\right) = \frac{4\pi^2}{c^2}\sigma_{yz}\sigma_{zy} \tag{30}$$

$$\sigma_{yy,zz} = \frac{\sigma_\perp + \sigma_\parallel}{2} \pm \frac{\sigma_\perp - \sigma_\parallel}{2}\cos 2\theta \tag{31}$$

$$\sigma_{yz,zy} = \frac{\sigma_\perp - \sigma_\parallel}{2}\sin 2\theta. \tag{32}$$

Here, θ defines the propagation direction of the SWs (figure 13(a)). The spectrum of the surface waves on the anisotropic metasurfaces was analyzed in [18, 19, 194]. In particular, it was shown that the polarization of the SWs on an anisotropic metasurface is hybrid and depends on the propagation direction (on angle θ) [195]. The pure TE- and TM-plasmons propagate along the principle axes of the metasurface when the right part of equation (30) vanishes. It occurs when $\theta = 0°, \pm 90°, 180°$.

For anisotropic metasurfaces it is possible to distinguish three regimes: (i) a capacitive metasurface when both $\mathrm{Im}[\sigma_\perp]$ and $\mathrm{Im}[\sigma_\parallel]$ are negative; (ii) a hyperbolic metasurface when $\mathrm{Im}[\sigma_\perp]\mathrm{Im}[\sigma_\parallel] < 0$; and (iii) an inductive metasurface when both $\mathrm{Im}[\sigma_\perp]$ and $\mathrm{Im}[\sigma_\parallel]$ are positive (see figure 13(c)). By

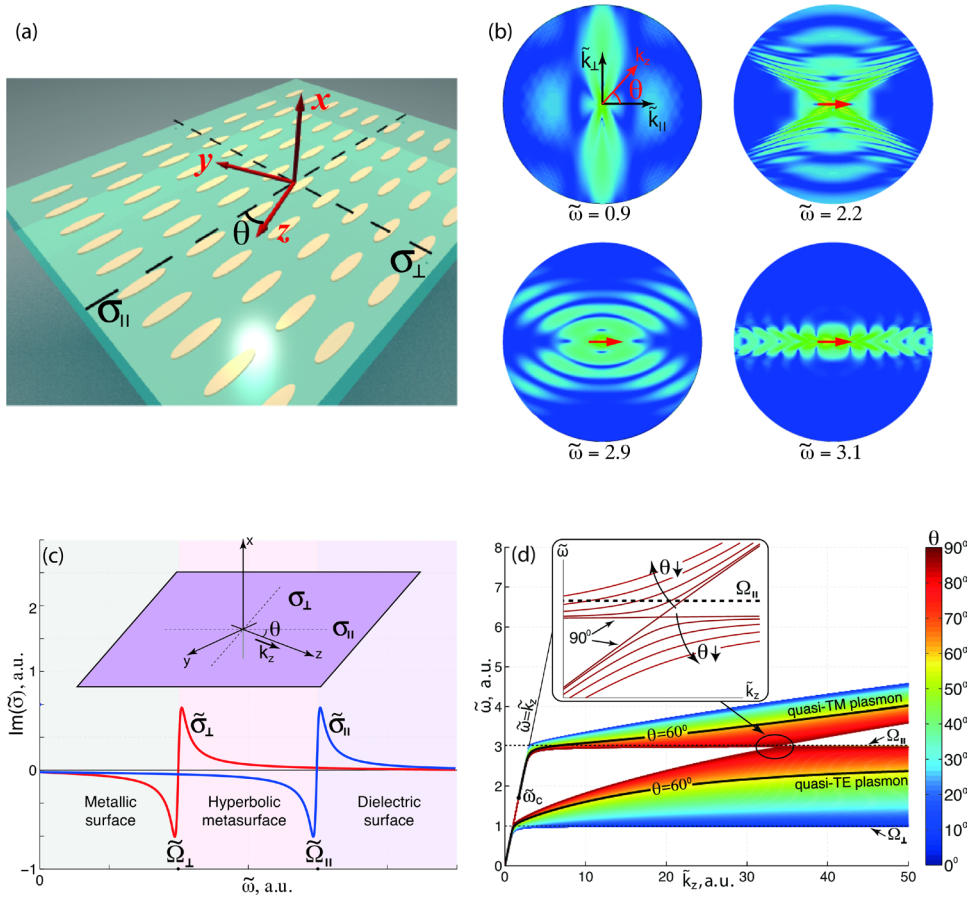

Figure 13. (a) A metasurface consisting of plasmonic anisotropic nanoparticles [18]. (b) Logarithmic maps of the electric field amplitude for four values of normalized frequency for the case when surface waves are excited by a point electric dipole. The dipole orientation is shown with the red arrow. (c) Frequency dependence of the imaginary parts of the conductivity tensor components. (d) Dependence of $\tilde{\omega}$ on $\tilde{k}_z$ for the surface waves on a hyperbolic metasurface for different propagation directions defined through angle θ. The two branches correspond to quasi-TM and quasi-TE surface plasmons. The inset shows the structure of dispersion curves at $\theta \approx 90°$. Reprinted figure with permission from [18], Copyright 2015 by the American Physical Society.

analogy with bulk metamaterials, transition between these regimes is often called a *topological transition* because it is accompanied by a change of isofrequency contour topology in the **k**-space [196]. The dispersion of TE- and TM-plasmons for different propagation directions is shown in figure 13(d). On anisotropic metasurfaces TE- and TM-plasmons can propagate simultaneously on the same frequency. It is feasible in the hyperbolic regime. The characteristic feature of the hyperbolic regime is the cross-shaped wave fronts when the SWs are excited by a point dipole placed in the vicinity of the metasurface (see figure 13(b) at $\tilde{\omega} = 2.2$ and 2.9). In the capacitive regime, the surface plasmon is weakly localized and behaves in similar way to light. This manifests in the intensity map similar to the point dipole in vacuum (figure 13(b) at $\tilde{\omega} = 0.9$). In the inductive regime at the frequencies close to topological transition one can observe strong anisotropic (one-dimensional) propagation of 2D SW (figure 13(b) at $\tilde{\omega} = 3.1$). This regime is also called *σ-near-zero* by an analogy with the *ε-near-zero* regime in metamaterials [197].

The spectra of resonant anisotropic metasurfaces were characterized in the radiofrequency, visible and near-IR ranges as reported in [198–200]. In [199] the metasurface consists of gold anisotropic (elliptically shaped) nanoparticles placed in a square lattice on a silica substrate. It was shown that in addition to the TE- and TM-plasmons, a nearly dispersionless mode exists. It appears due to the collective coupling of the quadrupole resonances of the plasmonic nanoparticles. A limit case of an anisotropic metasurface—an array of parallel metallic wires—was considered in [201, 202].

It is important to notice that equation (30) also describes the dispersion of 2D magnetoplasmons. The only difference is that the right part is proportional to the Hall conductivity which arises due to an external magnetic field applied perpendicularly to the metasurface. The spectrum of 2D magnetoplasmons is analyzed in [203]. The similar right part in equation (30) appears in the case of chiral metasurfaces due to the internal symmetry of the unit cell. Equation (30) is also valid in the case of a metasurface with a nonlocal electromagnetic response. The only adjustment is that we need to replace $\hat{\sigma}(\omega)$ by $\hat{\sigma}(\omega, \mathbf{k}_{||})$, where $\mathbf{k}_{||}$ is the in-plane wavevector.

The effective 2D conductivity tensor, taking into account spatial and time dispersion phenomena, can be calculated using Green's function formalism and lattice sums technique [204–207]. Within this approach all meta-atoms are replaced by point objects with electric and/or magnetic susceptibilities. This method allows one to take into account non-zero polarizability perpendicular to the metasurface, geometry of the unit cell, interaction between metaatoms, and effects of spatial

dispersion. This method is widely used for the analysis of visible and RF metasurfaces consisting of distinct metallic, point-like, or wire scatterers [208–213]. For high-index dielectric metasurfaces consisting of distinguishable scatterers, the lattice sum technique allows one to analyze dispersion of the surface waves in terms of coupled electric dipoles and magnetic dipoles, quadrupoles, and high order Mie resonances [214]. For very high-index dielectric metasurfaces, which are simply implemented at the radio frequencies, this approach works well because at the resonant frequencies of individual scatterers the metasurface remains subwavelength. In optics, for all-dielectric metasurfaces with a refractive index about 3.5 such a regime is almost unachievable and, therefore, different multipole resonances make a comparable contribution to the spectrum. Spectra of such metasurfaces are well described by the methods developed for photonic crystal slabs [215–218].

6. Conclusions and outlook

In this article we have discussed and provided a comprehensive overview of various types of surface waves in optics. We focus on their characteristics, materials' systems that support SWs, and the current status of both experimental and theoretical studies. Each of the SWs possesses unique features, such as high localization, directionality controlled by the dielectric environment, polarization, wavelength and unidirectional propagation enabled by an applied magnetic field, providing a wide variety of possibilities to manipulate light at the nanoscale. These properties can be significantly enhanced and extended by application of metamaterial platforms with deliberately tailored optical properties. Moreover, new phenomena and applications can be enabled by a combination of different types of surface waves, and here sophisticated metamaterial platforms can play a decisive role providing extra-properties on-demand. Major hurdles for the development of hybrid surface waves are encountered in the fabrication of metamaterial structures for the visible and near-infrared wavelength regions, where the periodicity and minimal features' sizes of metamaterials are still challenging for reproducible fabrication. Additionally, any metal inclusions contribute with undesired losses. We anticipate that hyperbolic and all-dielectric metamaterials and metasurfaces will play a major role in the near future. Also, the application of 2D materials such as graphene and hBN that are natural hyperbolic metamaterials for mid-IR seems to be very productive. The alliance of 2D materials with structured metamaterials can bring a conceptual platform flexible enough to accommodate SWs with extreme functionalities in broad frequency ranges. We believe that SWs can serve as a work horse for establishing a new field of *surface photonics*, not competing but complementing modern nanophotonics. Extended nomenclature of SWs can provide enough degrees of freedom to address the bottlenecks in various wavelength ranges with high potential for applications. One more direction which is foreseen as being a favorable testing ground of SWs applications is sensing, especially biosensing. Here, the confinement of SWs close to the interfaces can play a crucial role in high sensitivities, low limits of detection and universality towards different chemical and biological agents.

Acknowledgment

This work was supported by Villum Fonden DarkSILD project No. 11116 and Direktør Ib Henriksens Fond, Denmark. The authors are grateful to A P Slobozhanyuk for useful discussions. AAB acknowledges the Ministry of Education and Science of the Russian Federation (3.1668.2017/4.6 and 3.8891.2017/8.9) and RFBR (17-02-01234, 16-32-00248).

ORCID iDs

O Takayama https://orcid.org/0000-0003-3525-3262
A A Bogdanov https://orcid.org/0000-0002-8215-0445
A V Lavrinenko https://orcid.org/0000-0001-8853-2033

References

[1] Sinev I S, Bogdanov A A, Komissarenko F E, Frizyuk K S, Petrov M I, Mukhin I S, Makarov S V, Samusev A K, Lavrinenko A V and Iorsh I V 2017 Chirality Driven by Magnetic Dipole Response for Demultiplexing of Surface Waves *Laser Photon. Rev.* **11** 1700168
[2] Polo J and Lakhtakia A 2011 *Laser Photon. Rev.* **5** 234–46
[3] Takayama O, Shkondin E, Panah M E A, Repän T, Malureanu R, Jensen F and Lavrinenko A V 2016 Surface waves on metamaterials interfaces *10th Int. Congress on Advanced Electromagnetic Materials in Microwaves and Optics (metamaterials)* (IEEE) pp 199–201
[4] Barnes W L, Dereux A and Ebbesen T W 2003 *Nature* **424** 824–31
[5] Gollub J N, Smith D R, Vier D C, Perram T and Mock J J 2005 *Phys. Rev.* B **71** 195402
[6] D'yakonov M I 1988 *JETP* **67** 714–6
[7] Camley R E 1987 *Surf. Sci. Rep.* **7** 103–87
[8] Yeh P, Yariv A and Cho A Y 1978 *Appl. Phys. Lett.* **32** 104–5
[9] Tomlinson W J 1980 *Opt. Lett.* **5** 323–5
[10] Le Gall J, Olivier M and Greffet J J 1997 *Phys. Rev.* B **55** 10105
[11] Shen S, Narayanaswamy A and Chen G 2009 *Nano Lett.* **9** 2909–13
[12] Huber A, Ocelic N, Kazantsev D and Hillenbrand R 2005 *Appl. Phys. Lett.* **87** 81103
[13] Li P, Yang X, Maß T W W, Hanss J, Lewin M, Michel A K U, Wuttig M and Taubner T 2016 *Nat. Mater.* **15** 870–5
[14] Lagois J and Fischer B 1976 *Phys. Rev. Lett.* **36** 680
[15] Fischer B and Lagois J 1979 Surface exciton polaritons *Excitons* (Berlin: Springer) pp 183–210
[16] Hwang E H and Sarma S D 2007 *Phys. Rev.* B **75** 205418
[17] Mikhailov S A and Ziegler K 2007 *Phys. Rev. Lett.* **99** 16803
[18] Yermakov O Y, Ovcharenko A I, Song M, Bogdanov A A, Iorsh I V and Kivshar Y S 2015 *Phys. Rev.* B **91** 235423
[19] Gomez-Diaz J S, Tymchenko M and Alù A 2015 *Phys. Rev. Lett.* **114** 233901
[20] Jacob Z and Narimanov E E 2008 *Appl. Phys. Lett.* **93** 221109
[21] Kildishev A V, Boltasseva A and Shalaev V M 2013 *Science* **339** 1232009
[22] Takayama O *et al* 2017 private communication (arXiv1704.06108)
[23] Wang Z, Chong Y D, Joannopoulos J D and Soljačić M 2008 *Phys. Rev. Lett.* **100** 013905
[24] Maimistov A I and Lyashko E I 2016 *Opt. Spectrosc.* **121** 635–42
[25] Slobozhanyuk A, Mousavi S H, Ni X, Smirnova D, Kivshar Y S and Khanikaev A B 2017 *Nat. Photon.* **11** 130–6

[26] Wood R 1902 *Proc. Phys. Soc. Lond.* **18** 269
[27] Cai W and Shalaev V M 2010 *Optical Metamaterials* vol 10 (Berlin: Springer)
[28] Jahani S and Jacob Z 2016 *Nat. Nanotechnol.* **11** 23–36
[29] Yu N and Capasso F 2014 *Nat. Mater.* **13** 139–50
[30] Kittel C 1966 *Introduction to Solid State* vol 162 (New York: Wiley)
[31] Maier S A 2007 *Plasmonics: Fundamentals and Applications* (Berlin: Springer)
[32] West P R, Ishii S, Naik G V, Emani N K, Shalaev V M and Boltasseva A 2010 *Laser Photon. Rev.* **4** 795–808
[33] Naik G V, Liu J, Kildishev A V, Shalaev V M and Boltasseva A 2012 *Proc. Natl Acad. Sci.* **109** 8834–8
[34] Boltasseva A 2014 *MRS Bull.* **39** 461–8
[35] Law S, Podolskiy V and Wasserman D 2013 *Nanophotonics* **2** 1–28
[36] Sun J, Litchinitser N M and Zhou J 2014 *ACS Photon.* **1** 293–303
[37] Dai S *et al* 2014 *Science* **343** 1125–9
[38] Basov D N, Fogler M M and Garcia de Abajo F J 2016 *Science* **354** 195
[39] Low T, Chaves A, Caldwell J D, Kumar A, Fang N X, Avouris P, Heinz T F, Guinea F, Martin-Moreno L and Koppens F 2017 *Nat. Mater.* **16** 182–94
[40] Otto A 1968 *Z. Phys.* **216** 398–410
[41] Kretschmann E and Raether H 1968 *Z. Naturforsch.* A **23** 2135–6
[42] Zenhausern F, O'Boyle M P and Wickramasinghe H K 1994 *Appl. Phys. Lett.* **65** 1623–5
[43] Chen J *et al* 2012 *Nature* **487** 77–81
[44] Grandidier J, Des Francs G C, Massenot S, Bouhelier A, Markey L, Weeber J C and Dereux A 2010 *J. Microsc.* **239** 167–72
[45] Stegeman G I, Wallis R F and Maradudin A A 1983 *Opt. Lett.* **8** 386–8
[46] Economou E 1969 *Phys. Rev.* **182** 539–54
[47] Kinsey N, Ferrera M, Shalaev V M and Boltasseva A 2015 *J. Opt. Soc. Am.* B **32** 121
[48] Maier S A and Atwater H A 2005 *J. Appl. Phys.* **98** 011101
[49] Pitarke J M, Silkin V M, Chulkov E V and Echenique P M 2007 *Rep. Prog. Phys.* **70** 1–87
[50] Homola J, Yee S S and Gauglitz G 1999 *Sensors Actuators* B **54** 3–15
[51] Anker J N, Hall W P, Lyandres O, Shah N C, Zhao J and Van Duyne R P 2008 *Nat. Mater.* **7** 442–53
[52] Adato R, Aksu S and Altug H 2015 *Mater. Today* **18** 436–46
[53] Haas J and Mizaikoff B 2016 *Annu. Rev. Anal. Chem.* **9** 45–68
[54] Lal S, Link S and Halas N J 2007 *Nat. Photon.* **1** 641–8
[55] Berini P 2009 *Adv. Opt. Photon.* **1** 484–588
[56] Han Z and Bozhevolnyi S I 2012 *Rep. Prog. Phys.* **76** 16402
[57] MacDonald K F and Zheludev N I 2010 *Laser Photon. Rev.* **4** 562–7
[58] Kauranen M and Zayats A V 2012 *Nat. Photon.* **6** 737–48
[59] Juan M L, Righini M and Quidant R 2011 *Nat. Photon.* **5** 349–56
[60] Bogdanov A A and Suris R A 2011 *Phys. Rev.* B **83** 125316
[61] Williams B S, Kumar S, Callebaut H, Hu Q and Reno J L 2003 *Appl. Phys. Lett.* **83** 2124
[62] Taminiau T H, Stefani F D, Segerink F B and Van Hulst N F 2008 *Nat. Photon.* **2** 234–7
[63] Lu D and Liu Z 2012 *Nat. Commun.* **3** 1205
[64] Smith D R, Pendry J B and Wiltshire M C K 2004 *Science* **305** 788–92
[65] Shalaev V M 2007 *Nat. Photon.* **1** 41–8
[66] Veselago V G 1968 *Sov. Phys.—Usp* **10** 509
[67] Sarychev A K, Shvets G and Shalaev V M 2006 *Phys. Rev.* E **73** 36609
[68] Ruppin R 2000 *Phys. Lett.* A **277** 61–4
[69] Ruppin R 2001 *J. Phys.: Condens. Matter* **13** 1811
[70] Darmanyan S A, Neviere M and Zakhidov A A 2003 *Opt. Commun.* **225** 233–40
[71] Shadrivov I V, Sukhorukov A A, Kivshar Y S, Zharov A A, Boardman A D and Egan P 2004 *Phys. Rev.* E **69** 16617
[72] Boardman A D, Velasco L, King N and Rapoport Y 2005 *JOSA* B **22** 1443–52
[73] Tsakmakidis K L, Hermann C, Klaedtke A, Jamois C and Hess O 2006 *Phys. Rev.* B **73** 85104
[74] Kats A V, Savel'ev S, Yampol'skii V A and Nori F 2007 *Phys. Rev. Lett.* **98** 73901
[75] Huidobro P A, Shen X, Cuerda J, Moreno E, Martin-Moreno L, Garcia-Vidal F J, Cui T J and Pendry J B 2014 *Phys. Rev.* X **4** 021003
[76] Liu N, Mukherjee S, Bao K, Li Y, Brown L V, Nordlander P and Halas N J 2012 *ACS Nano* **6** 5482–8
[77] Liu N, Mukherjee S, Bao K, Brown L V, Dorfmüller J, Nordlander P and Halas N J 2012 *Nano Lett.* **12** 364–9
[78] Paniagua-Domínguez R, Sánchez-Gil J A, Albella P, Sáiz J M, González F and Moreno F 2010 *Metamaterials* **4** 201–6
[79] Paniagua-Dominguez R, Froufe-Pérez L S, Sáenz J J and Sánchez-Gil J A 2015 *Phys. Rev.* B **91** 235120
[80] Walker D B, Glytsis E N and Gaylord T K 1998 *JOSA* A **15** 248–60
[81] Takayama O, Crasovan L C, Johansen S K, Mihalache D, Artigas D and Torner L 2008 *Electromagnetics* **28** 126–45
[82] Takayama O, Crasovan L, Artigas D and Torner L 2009 *Phys. Rev. Lett.* **102** 043903
[83] Torner L, Torres J P and Mihalache D 1993 *IEEE Photon. Technol. Lett.* **5** 201–3
[84] Torner L, Torres J P, Ojeda C and Mihalache D 1995 *J. Lightwave Technol.* **13** 2027–33
[85] Takayama O, Artigas D and Torner L 2014 *Nat. Nanotechnol.* **9** 419–24
[86] Noginov M A 2014 *Nat. Nanotechnol.* **9** 414–5
[87] Artigas D and Torner L 2005 *Phys. Rev. Lett.* **94** 013901
[88] Takayama O, Artigas D and Torner L 2012 *Opt. Lett.* **37** 4311
[89] Matsui T 2015 *Appl. Phys. Express* **8** 072601
[90] Averkiev N S and Dyakonov M I 1990 *Opt. Spectrosc.* **68** 653–5
[91] Darinskii A N 2001 *Crystallogr. Rep.* **46** 842–4
[92] Alshits V I and Lyubimov V N 2002 *Phys. Solid State* **44** 1988–92
[93] Furs A N, Galynsky V M and Barkovsky L M 2005 *J. Phys. A. Math. Gen.* **38** 8083
[94] Takayama O, Nikitin A Y, Martin-Moreno L, Torner L and Artigas D 2011 *Opt. Express* **19** 6339
[95] Takayama O, Artigas D and Torner L 2012 *Opt. Lett.* **37** 1983–5
[96] Nelatury S R, Polo J A Jr and Lakhtakia A 2008 *Electromagnetics* **28** 162–74
[97] Crasovan L C, Takayama O, Artigas D, Johansen S K, Mihalache D and Torner L 2006 *Phys. Rev.* B **74** 155120
[98] Vuković S M, Miret J J, Zapata-Rodriguez C J and Jakšić Z 2012 *Phys. Scr.* **T149** 014041
[99] High A A, Devlin R C, Dibos A, Polking M, Wild D S, Perczel J, de Leon N P, Lukin M D and Park H 2015 *Nature* **522** 192–6
[100] Poddubny A, Iorsh I V, Belov P and Kivshar Y 2013 *Nat. Photon.* **7** 948–57
[101] Ferrari L, Wu C, Lepage D, Zhang X and Liu Z 2015 *Prog. Quantum Electron.* **40** 1–40
[102] Shekhar P, Atkinson J and Jacob Z 2014 *Nano Convergence* **1** 14
[103] Zapata-Rodriguez C J, Miret J J, Vuković S and Belić M R 2013 *Opt. Express* **21** 19113–27
[104] Narimanov E E 2014 *Phys. Rev.* X **4** 1–13

[105] Gao W L, Fang F Z, Liu Y M and Zhang S 2015 *Light Sci. Appl.* **4** e328
[106] Yan W, Shen L, Ran L and Kong J A 2007 *JOSA* A **24** 530–5
[107] Li R, Cheng C, Ren F F, Chen J, Fan Y X, Ding J and Wang H T 2008 *Appl. Phys. Lett.* **92** 141115
[108] Chern R L 2013 *J. Opt.* **15** 75702
[109] Pattanayak D N and Birman J L 1981 *Phys. Rev.* B **24** 4271
[110] Puri A, Pattanayak D N and Birman J L 1982 *JOSA* **72** 938–42
[111] Engheta N and Pelet P 1991 *Opt. Lett.* **16** 723–5
[112] Chiu K W and Quinn J J 1972 *Phys. Rev. Lett.* **29** 600
[113] Brion J J, Wallis R F, Hartstein A and Burstein E 1972 *Phys. Rev. Lett.* **28** 1455
[114] Yu Z, Veronis G, Wang Z and Fan S 2008 *Phys. Rev. Lett.* **100** 23902
[115] Remer L, Mohler E, Grill W and Lüthi B 1984 *Phys. Rev.* B **30** 3277
[116] Khurgin J B 2006 *Appl. Phys. Lett.* **89** 251115
[117] Sepulveda B, Lechuga L M and Armelles G 2006 *J. Lightwave Technol.* **24** 945
[118] Montoya J, Parameswaran K, Hensley J, Allen M and Ram R 2009 *J. Appl. Phys.* **106** 23108
[119] Temnov V V, Armelles G, Woggon U, Guzatov D, Cebollada A, Garcia-Martin A, Garcia-Martin J M, Thomay T, Leitenstorfer A and Bratschitsch R 2010 *Nat. Photon.* **4** 107–11
[120] Furs A N and Barkovsky L M 2007 *J. Phys. A: Math. Theor.* **40** 309
[121] Furs A N and Barkovsky L M 2008 *Electromagnetics* **28** 146–61
[122] Furs A N and Barkovsky L M 2003 *Tech. Phys.* **48** 385–92
[123] Shen W Z and Li Z Y 1992 *Phys. Rev.* B **46** 14205
[124] Zhao Y, Wan W L and Wang X Z 1999 *Phys. Lett.* A **255** 178–82
[125] Boardman A, King N, Rapoport Y and Velasco L 2005 *New J. Phys.* **7** 191
[126] Joannopoulos J D, Johnson S G, Winn J N and Meade R D 2008 *Photonic Crystals: Molding the Flow of Light* 2nd edn (New Jersey: Princeton University Press)
[127] Yariv A and Yeh P 1977 *J. Opt. Soc. Am.* **67** 438
[128] Vinogradov A P, Dorofeenko A, Merzlikin A and Lisyansky A 2010 *Usp. Fiz. Nauk* **180** 249
[129] Tamm I 1932 *Phys. Z. Sov. Union* **1** 733–5
[130] Ohno H, Mendez E E, Brum J A, Hong J M, Agulló-Rueda F, Chang L L and Esaki L 1990 *Phys. Rev. Lett.* **64** 2555
[131] Liscidini M and Sipe J E 2009 *J. Opt. Soc. Am.* B **26** 279–89
[132] Yu L, Barakat E, Sfez T, Hvozdara L, Di Francesco J and Herzig H P 2014 *Light Sci. Appl.* **3** e124
[133] Sinibaldi A, Danz N, Descrovi E, Munzert P, Schulz U, Sonntag F, Dominici L and Michelotti F 2012 *Sensors Actuators* B **174** 292–8
[134] Vukovic S M, Shadrivov I V and Kivshar Y S 2009 *Appl. Phys. Lett.* **95** 041902
[135] Xiang Y, Guo J, Dai X, Wen S and Tang D 2014 *Opt. Express* **22** 3054
[136] Kossel D 1966 *J. Opt. Soc. Am.* **56** 1434
[137] Robertson W M 1999 *J. Lightwave Technol.* **17** 2013
[138] Ramos-Mendieta F and Halevi P 1999 *Phys. Rev.* B **59** 15112
[139] Zhou H, Yang G, Wang K, Long H and Lu P 2010 *Opt. Lett.* **35** 4112–4
[140] Fang Y T, Chen L K, Zhu N and Zhou J 2013 *IET Optoelectron.* **7** 9–13
[141] Brand S, Kaliteevski M A and Abram R A 2009 *Phys. Rev.* B **79** 85416
[142] Iorsh I V, Orlov A, Belov P and Kivshar Y 2011 *Appl. Phys. Lett.* **99** 151914
[143] Bogdanov A A and Suris R A 2012 *JETP Lett.* **96** 49–55
[144] Golenitskii K Y, Koshelev K L and Bogdanov A A 2016 *Phys. Rev.* A **94** 43815
[145] Robertson W M, Arjavalingam G, Meade R D, Brommer K D, Rappe A M and Joannopoulos J D 1993 *Opt. Lett.* **18** 528–30
[146] Wang B, Dai W, Fang A, Zhang L, Tuttle G, Koschny T and Soukoulis C M 2006 *Phys. Rev.* B **74** 195104
[147] Foteinopoulou S, Kafesaki M, Economou E N and Soukoulis C M 2007 *Phys. Rev.* B **75** 245116
[148] Foteinopoulou S, Kenanakis G, Katsarakis N, Tsiapa I, Kafesaki M, Economou E N and Soukoulis C M 2007 *Appl. Phys. Lett.* **91** 214102
[149] Plotnik Y *et al* 2013 *Nat. Mater.* **13** 57–62
[150] Meade R D, Brommer K D, Rappe A M and Joannopoulos J D 1991 *Phys. Rev.* B **44** 10961
[151] Ishizaki K and Noda S 2009 *Nature* **460** 367–70
[152] Pulsifer D P, Faryad M and Lakhtakia A 2013 *Phys. Rev. Lett.* **111** 243902
[153] Pulsifer D P, Faryad M, Lakhtakia A, Hall A S and Liu L 2014 *Opt. Lett.* **39** 2125–8
[154] Ciumac M, Baboiu D M and Mihalache D 1994 *Opt. Commun.* **111** 548–55
[155] Kaliteevski M, Iorsh I V, Brand S, Abram R A, Chamberlain J M, Kavokin A V and Shelykh I A 2007 *Phys. Rev.* B **76** 165415
[156] Sasin M E *et al* 2010 *Superlattices Microstruct.* **47** 44–9
[157] Symonds C, Lheureux G, Hugonin J P, Greffet J J, Laverdant J, Brucoli G, Lemaitre A, Senellart P and Bellessa J 2013 *Nano Lett.* **13** 3179–84
[158] Lheureux G, Azzini S, Symonds C, Senellart P, Lemaitre A, Sauvan C, Hugonin J P, Greffet J J and Bellessa J 2015 *ACS Photon.* **2** 842–8
[159] Azzini S, Lheureux G, Symonds C, Benoit J M, Senellart P, Lemaitre A, Greffet J J, Blanchard C, Sauvan C and Bellessa J 2016 *ACS Photon.* **3** 1776–81
[160] Das R, Srivastava T and Jha R 2014 *Opt. Lett.* **39** 896–9
[161] Sun X C, He C, Liu X P, Lu M H, Zhu S N and Chen Y F 2017 *Prog. Quantum Electron.* **55** 52–73
[162] Lu L, Joannopoulos J D and Soljačić M 2016 *Nat. Phys.* **12** 626–9
[163] Lu L, Joannopoulos J D and Soljačić M 2014 *Nat. Photon.* **8** 821–9
[164] Haldane F D M and Raghu S 2008 *Phys. Rev. Lett.* **100** 13904
[165] Raghu S and Haldane F D M 2008 *Phys. Rev.* A **78** 33834
[166] Wang Z, Chong Y, Joannopoulos J D and Soljačić M 2009 *Nature* **461** 772
[167] Fang K, Yu Z and Fan S 2012 *Nat. Photon.* **6** 782–7
[168] Khanikaev A B, Hossein Mousavi S, Tse W K, Kargarian M, MacDonald A H and Shvets G 2013 *Nat. Mater.* **12** 233–9
[169] Slobozhanyuk A P, Khanikaev A B, Filonov D S, Smirnova D A, Miroshnichenko A E and Kivshar Y S 2016 *Sci. Rep.* **6** 22270
[170] Slobozhanyuk A, Shchelokova A V, Ni X, Mousavi S H, Smirnova D A, Belov P A, Alù A, Kivshar Y S and Khanikaev A B 2017 private communication (arXiv1705.07841)
[171] Cheng X, Jouvaud C, Ni X, Mousavi S H, Genack A Z and Khanikaev A B 2016 *Nat. Mater.* **15** 542–8
[172] Ma T and Shvets G 2016 *New J. Phys.* **18** 25012
[173] Gangaraj S A H, Nemilentsau A and Hanson G W 2016 *Sci. Rep.* **6** 30055
[174] Chern R L and Yu Y Z 2017 *Opt. Express* **25** 11801–12
[175] Lu L, Fang C, Fu L, Johnson S G, Joannopoulos J D and Soljačić M 2016 *Nat. Phys.* **12** 337–40
[176] Varatharajah P, Heatley D R, Wright E M, Aceves A and Moloney J V 1988 *Opt. Lett.* **13** 690–2
[177] Mihalache D, Mazilu D and Delion D 1992 *Phys. Rev.* A **46** 4449
[178] Bradley P J and De Angelis C 1996 *Opt. Commun.* **130** 205–18
[179] Iorsh I V, Belov P A, Zharov A A, Shadrivov I V and Kivshar Y S 2012 *Phys. Rev.* A **86** 23819

[180] Iorsh I, Shadrivov I V, Belov P A and Kivshar Y S 2012 *Phys. Status Solidi (RRL)-Rapid Res. Lett.* **6** 43–5
[181] Torner L, Torres J P, Lederer F, Mihalache D, Baboiu D M and Ciumac M 1993 *Electron. Lett.* **29** 1186–8
[182] Torres J P, Torner L, Lederer F, Mihalache D, Baboiu D M and Ciumac M 1994 *JOSA* B **11** 983–5
[183] Kapitanova P V, Ginzburg P, Rodríguez-Fortuno F J, Filonov D S, Voroshilov P M, Belov P A, Poddubny A N, Kivshar Y S, Wurtz G A and Zayats A V 2014 *Nat. Commun.* **5** 3226
[184] Castellanos-Gomez A 2016 *Nat. Photon.* **10** 202–4
[185] Munk B A 2000 *Frequency Selective Surfaces* (New York: Wiley)
[186] Glybovski S B, Tretyakov S A, Belov P A, Kivshar Y S and Simovski C R 2016 *Phys. Rep.* **634** 1–72
[187] Stern F 1967 *Phys. Rev. Lett.* **18** 546–8
[188] Falko V I and Khmelnitskii D E 1989 *Zh. Eksp. Teor. Fiz* **95** 1988–92
[189] Sievenpiper D, Zhang L and Yablonovitch E 1999 High-impedance electromagnetic ground planes *1999 IEEE MTT-S Int. Microwave Symp. Digest (Cat. No.99CH36282) vol* 4 pp 1529–32 (IEEE)
[190] Costa F, Luukkonen O, Simovski C R, Monorchio A, Tretyakov S A and De Maagt P M 2011 *IEEE Trans. Antennas Propag.* **59** 3588–96
[191] Chshelokova A V, Kapitanova P V, Poddubny A N, Filonov D S, Slobozhanyuk A P, Kivshar Y S and Belov P A 2012 *J. Appl. Phys.* **112** 73116
[192] Liu Y and Zhang X 2013 *Appl. Phys. Lett.* **103** 141101
[193] Talebi N, Ozsoy-Keskinbora C, Benia H M, Kern K, Koch C T and van Aken P A 2016 *ACS Nano* **10** 6988–94
[194] Nemilentsau A, Low T and Hanson G 2016 *Phys. Rev. Lett.* **116** 66804
[195] Yermakov O Y, Ovcharenko A I, Bogdanov A A, Iorsh I V, Bliokh K Y and Kivshar Y S 2016 *Phys. Rev.* B **94** 75446
[196] Krishnamoorthy H N, Jacob Z, Narimanov E, Kretzschmar I and Menon V M 2012 *Science* **336** 205–9
[197] Engheta N 2013 *Science* **340** 286–7
[198] Anghinolfi L, Mattera L, Canepa M and Bisio F 2012 *Phys. Rev.* B **85** 235426
[199] Samusev A *et al* 2017 private communication (arXiv1705.06078)
[200] Yang Y, Jing L, Shen L, Wang Z, Zheng B, Wang H, Li E, Shen N H, Koschny T, Soukoulis C M *et al* 2017 *NPG Asia Mater.* **9** e428
[201] Macfarlane G G 1946 *J. Inst. Electr. Eng.* **93** 1523–7
[202] Razafindrakoto R, Rousseau E, Felbacq D and Kling E 2014 Confined modes on a meta-surface *SPIE Nanoscience Engineering (International Society for Optics and Photonics)* p 917203
[203] Iorsh I V, Shadrivov I, Belov P and Kivshar Y 2013 *JETP Lett.* **97** 249
[204] Tretyakov S 2003 *Analytical Modeling in Applied Electromagnetics* (Boston: Artech House)
[205] McPhedran R C, Nicorovici N A, Botten L C and Grubits K A 2000 *J. Math. Phys.* **41** 7808
[206] Nicorovici N A, McPhedran R C and Ke-Da B 1995 *Phys. Rev.* E **51** 690–702
[207] Chin S, Nicorovici N and McPhedran R 1994 *Phys. Rev.* E **49** 4590–602
[208] Koenderink A F, de Waele R, Prangsma J C and Polman A 2007 *Phys. Rev.* B **76** 201403
[209] García de Abajo F J and Sáenz J J 2005 *Phys. Rev. Lett.* **95** 233901
[210] Backes T D and Citrin D S 2008 *IEEE J. Sel. Top. Quantum Electron.* **14** 1530–5
[211] Simsek E 2009 *Plasmonics* **4** 223–30
[212] Mousavi S H, Khanikaev A B, Neuner B, Fozdar D Y, Corrigan T D, Kolb P W, Drew H D, Phaneuf R J, Alù A and Shvets G 2011 *Opt. Express* **19** 22142–55
[213] Liang F, Hanson G W, Yakovlev A B, Lovat G, Burghignoli P, Araneo R and Hassani Gangaraj S A 2016 *IEEE Trans. Antennas Propag.* **64** 167–78
[214] Swiecicki S D and Sipe J E 2017 *Phys. Rev.* B **95** 195406
[215] Andreani L C and Gerace D 2006 *Phys. Rev.* B **73** 235114
[216] Johnson S G, Fan S, Villeneuve P R, Joannopoulos J D and Kolodziejski L A 1999 *Phys. Rev.* B **60** 5751
[217] Tikhodeev S G, Yablonskii A L, Muljarov E A, Gippius N A and Ishihara T 2002 *Phys. Rev.* B **66** 045102
[218] Weiss T, Schäferling M, Giessen H, Gippius N A, Tikhodeev S G, Langbein W and Muljarov E A 2017 *Phys. Rev.* B **96** 45129